Graduate School ETD Form 9
(Revised 12/07)

PURDUE UNIVERSITY
GRADUATE SCHOOL
Thesis/Dissertation Acceptance

This is to certify that the thesis/dissertation prepared

By Jaya Sangita Malladi

Entitled MODELING THE INTERDEPENDENCE OF ELECTROCHEMICAL AND MECHANICAL PROPERTIES IN PER SULFONATE ACID PROTON EXCHANGE MEMBRANES

For the degree of Master of Science in Mechanical Engineering

Is approved by the final examining committee:

Alan S. Jones
Chair

Jie Chen

Jian Xie

To the best of my knowledge and as understood by the student in the *Research Integrity and Copyright Disclaimer (Graduate School Form 20)*, this thesis/dissertation adheres to the provisions of Purdue University's "Policy on Integrity in Research" and the use of copyrighted material.

Approved by Major Professor(s): Alan S. Jones

Approved by: Jie Chen 12/09/2010
Head of the Graduate Program Date

Graduate School Form 20
(Revised 9/10)

PURDUE UNIVERSITY
GRADUATE SCHOOL

Research Integrity and Copyright Disclaimer

Title of Thesis/Dissertation:

MODELING THE INTERDEPENDENCE OF ELECTROCHEMICAL AND MECHANICAL PROPERTIES IN PER SULFONATE ACID PROTON EXCHANGE MEMBRANES

For the degree of Master of Science in Mechanical Engineering

I certify that in the preparation of this thesis, I have observed the provisions of *Purdue University Executive Memorandum No. C-22,* September 6, 1991, *Policy on Integrity in Research.**

Further, I certify that this work is free of plagiarism and all materials appearing in this thesis/dissertation have been properly quoted and attributed.

I certify that all copyrighted material incorporated into this thesis/dissertation is in compliance with the United States' copyright law and that I have received written permission from the copyright owners for my use of their work, which is beyond the scope of the law. I agree to indemnify and save harmless Purdue University from any and all claims that may be asserted or that may arise from any copyright violation.

M. Jaya Sangita

Printed Name and Signature of Candidate

12/09/2010

Date (month/day/year)

*Located at http://www.purdue.edu/policies/pages/teach_res_outreach/c_22.html

MODELING THE INTERDEPENDENCE OF ELECTROCHEMICAL AND MECHANICAL PROPERTIES IN PER SULFONATE ACID PROTON EXCHANGE MEMBRANES

A Thesis
Submitted to the Faculty
of
Purdue University
by
Jaya Sangita Malladi

In Partial Fulfillment of the
Requirements for the Degree
of
Master of Science in Mechanical Engineering

May 2011
Purdue University
Indianapolis, Indiana

ACKNOWLEDGMENTS

I would like to gratefully acknowledge my advisor Prof. Alan S. Jones, for his guidance, support, and advice during my graduate research and thesis work.

I am thankful to my committee members Prof Jian Xie, Prof. Jie Chen and Prof. Hazim El- Mounayri for their time and insight during the completion of the thesis work.

I would also like to thank Ms. Rongrong Chen of the Lugar Center Lab and my fellow students at the Mechatronics laboratory and Lugar center Laboratory for their help and engaging discussions. I would like thank Emily Tung for collecting some of the data.

I am also thankful to Graduate Coordinator Valerie Lim Diemer and Ginger Lauderback for assisting me in formatting of my thesis.

Finally, I am thankful to my husband and family members for their advice and support.

TABLE OF CONTENTS

Page

LIST OF TABLES

LIST OF FIGURES

Figure Page

Figure Page

ABSTRACT

Malladi, Jaya Sangita. M.S.M.E., Purdue University, May 2011. Modeling the Interdependence of Electrochemical and Mechanical Properties in Per Sulphonate Acid Proton Exchange Membranes. Major Professor: Alan Jones.

Proton exchange membrane fuel cells (PEMFC's) offer an attractive alternative energy resource over traditional fossil fuels. The advantages such as high power density, relatively quick start-up, rapid response to varying loads and low operating temperatures make it a preferred technology option compared to other alternative energy sources. Nafion® by DuPont plays an integral role in the success of PEM fuel cells due to its high proton conductivity and high chemical and thermal stability. This research project aims to study the effect of mechanical and hygro-thermal stresses on the mechanical performance and proton conductivity of the membrane by subjecting it to realistic operating conditions such as those encountered in an automobile.

In this thesis, the time-dependent behavior of the membrane has been modeled using a Prony series and the change in the conductivity due to mechanical loading was experimentally measured. The modeling of both electrochemical and mechanical properties can further be used in studying the degradation properties of the membrane and should guide the development of better membrane materials. Visco-elastic stress relaxation theory has been used in modeling the time-dependent behavior of the specimen. The EIS spectrum has been analyzed using a non-linear least squares method and an equivalent circuit method was also used to fit the spectra.

This project was conducted in three phases. In the first phase a novel test facility was built to perform the experiments. A conductivity measurement test cell that measured the proton conductivity of a membrane was modeled and manufactured. The second phase included the design of different experiments that helped in modeling the interdependence of electrochemical and mechanical properties of the membrane. In this process**,** three series of experiments that tested the electrochemical and mechanical properties of the specimen were conducted. The membrane was held at constant strain and the through plane impedance was measured at different times during the test, specifically before and after stretching at ambient and varying environmental conditions. The membrane was also subjected to both mechanical and hygro-thermal loading conditions during the test. In the third phase, time-dependant mathematical model for the changes in the material properties were developed.

The experimental apparatus thus tested the mechanical and electrochemical properties of the membrane simultaneously while the specimen was being subjected to constant mechanical and varying hygro-thermal conditions. Since the testing method is a novel procedure, the reliability and repeatability of the experimental facility has been verified before conducting the experiments. The experimental apparatus can further be used to test the membrane at varying strain rates and different hygro-thermal loading conditions in a consistent manner. The model developed can be used to analyze the degradation behavior of membrane and also to build better fabrication methods and membrane materials in future.

1. INTRODUCTION

1.1 Motivation for Fuel Cells

Depletion of fossil fuels in the past few decades and emission of harmful gases from the fuel has led society to actively look for alternative energy systems. Perfluorosulphonate acid (PFSA) based proton exchange membrane fuel cell systems are emerging as a promising resource for alternative energy systems. The need to control the air pollutants emitted by the fossil fuel technologies, the ever rising oil prices and environmental challenges such as global warming pose a strong need for a clean and economically viable technology such as the PEM technology [1, 2]. The fact the PEM fuel cells produce little or no harmful emissions make it an environmentally friendly option compared to internal combustion engine technologies [2 and 3]. High power density at low operating temperature [7] made the PFSA based PEM fuel cell a preferred candidate especially for transportation applications.

The applications of Polymer electrolyte membrane fuel cells (PEMFC's) in various fields have been increasing tremendously. They are being used in both stationary and portable power generation [1] along with widespread use in transportation industry. Typical applications of PEMFC's include cars, motorbikes, buses, locomotives, forklifts, light aircraft and UAVs and decentralized power generation. High efficiency and zero emission of harmful gases have been the major factors driving the PEMFC's to emerge as a promising source of alternative energy to the internal combustion engines [2]. Refueling PEM fuel cell vehicles is much faster as compared to battery operated vehicles and there is also no frequent recharging when compared to the latter.

Smaller fuel cells (power < 1 KW) are also being considered as an alternative to consumer electronics such as cell phones, laptop computers, cameras, and music players [1]. Their usage in portable power generation is also increasing as they operate for longer times (due to absence of heat and noise) when compared to internal combustion generators [18]. Their usage in military and space applications is also being increased. A few example applications include telecommunications, navigation systems, soldier power, ocean sensors, transponders, and NASA's space program (Project Gemini) [1, 6].

1.2 Fuel Cell – Operation and Types

A fuel cell is an electrochemical device that converts fuel energy into electrical energy. A single fuel cell, shown in Figure 1.1, is comprised of an anode, cathode, and electrolyte [12].

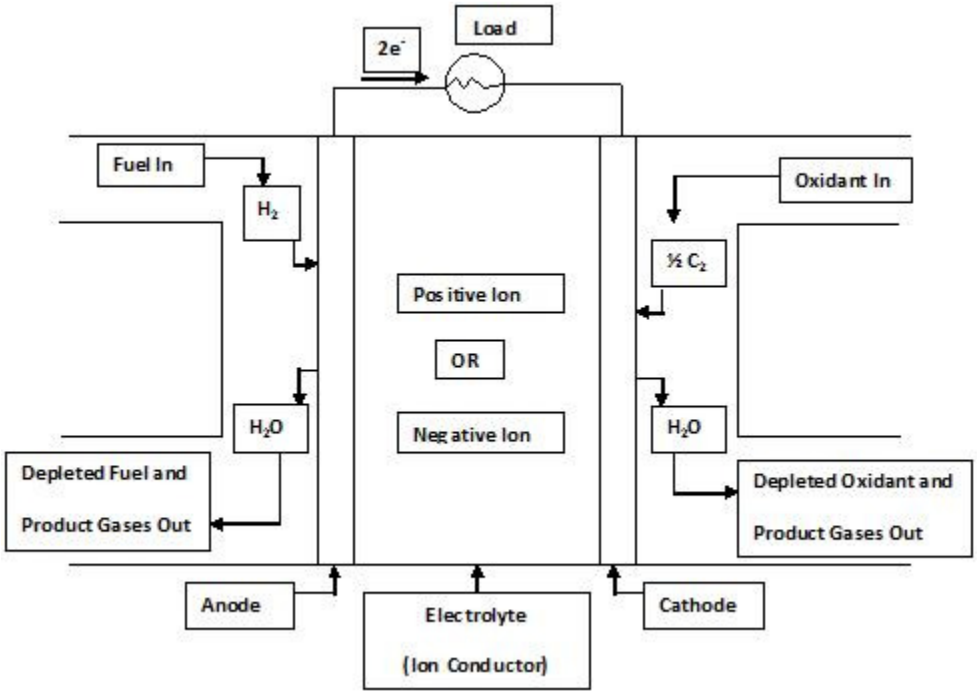

Figure 1.1 Schematic of a single fuel cell [12]

Typically, a fuel is fed into the cell at the anode and air is fed into the cell at the cathode. In a simple acid electrolyte fuel cell, the fuel is H_2 gas. The H_2 gas de- ionizes into electrons and protons (H^+ ions) in presence of an anode catalyst. The protons are conducted through the electrolyte while the electrons pass through an outer circuit towards the cathode. At the cathode the protons and electrons react with the oxidant supply (air or oxygen) to form water or carbon-dioxide. Figure 1.2 shows a fuel cell stack with possible electrolytes.

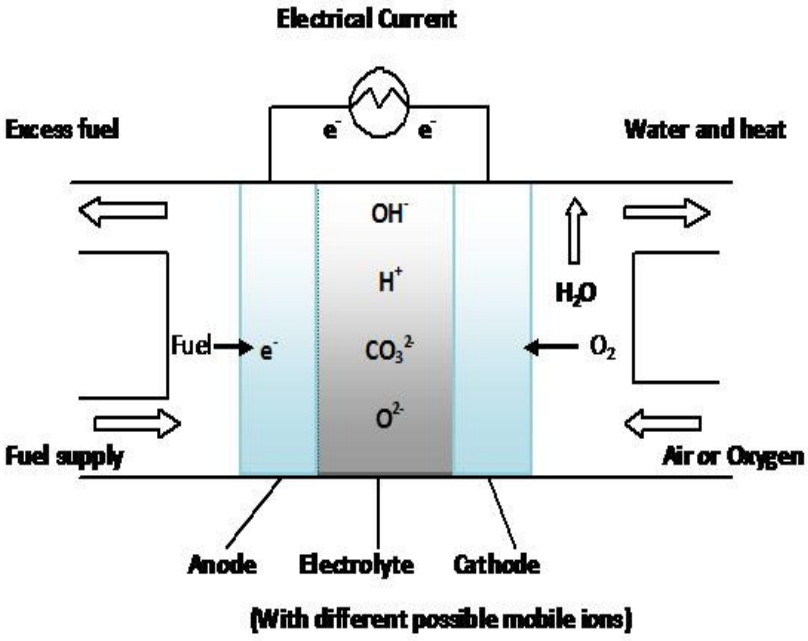

Figure 1.2 Fuel cell stack [9]

The fundamental chemical reactions that occur at the anode and cathode are the following:

Reaction at Anode:

$$2H_2 \longrightarrow 4H^+ + 4e^-$$

Reaction at Cathode:

$$O_2 + 4e^- + 4H^+ \longrightarrow 2H_2O$$

The gaseous fuel (generally H_2 gas) supplied to anode, splits into protons and electrons. The protons are transferred through the electrolyte combine with oxygen supplied at cathode while the electrons join from an external circuit to produce water and heat [12 and 22]. The electrochemical energy stored in the reactants drive the reaction while the electrons travelling from outer circuit generate the electrical energy [30]. For the above reactions to take place the electrons must pass through the outer circuit therefore, the electrolyte material must be electrically insulating.

The electrolyte has three requirements. First it must prevent the mixing of the anode and cathode gasses. Second it should only allow the flow of protons or ions through it, and finally it must act as an electronic insulator preventing the electrons or free ions from interrupting the reactions at the electrodes. The electrolyte of a PEM fuel cell is an ionomer, essentially a polymer in the form of a thin permeable sheet. Since it is a solid it does not leak which is a common problem with liquid electrolytes. A solid electrolyte fuel cell is cheaper to manufacture as it makes the sealing of anode and cathode gases much easier. Another major advantage of a solid electrolyte is, it increases the durability of the stack and cell as it is less subjected to corrosion compared to liquid electrolytes [6]. Polymer Electrolyte membrane fuel cells operate at low temperatures (around 80˚C) with an efficiency of about 40-50% making them suitable for automobile applications [9].

The other important components of a fuel cell are the gas channel and gas diffusion media (GDM). While the gas channel maintains the reactant and product flow, the GDM which is basically a carbon paper, maintains the transport of reactants and products between the catalyst layers and the gas channel. The GDM also maintains the electron flow and heat transfer between the reaction sites (catalyst layers) and bipolar plates. The catalyst layers are usually employed to speed up the electrochemical reactions at the electrodes [12]. These catalysts are usually very thin coating of platinum on a cloth or a carbon paper. The coated side of the catalyst faces the electrolyte and its surface is made rough and porous so that maximum area of the catalyst can be exposed to the

reactants. The other important components of a fuel cell stack include humidifiers and cooling plates which are required to remove the reaction heat and maintain the fuel cell at the required operating temperature [17].

Fuel cells are classified into many different types depending on the electrolyte substance (solid or liquid). The main electrolytes include molten carbonate, phosphoric acid, alkali, proton exchange membrane (PEM) and solid oxide. Among these different types, the PEM and solid oxide are solid electrolytes while the rest are liquid. The operating temperature and fuel supplied to a fuel cell depend on the type of electrolyte being used in it. Depending on the operating temperature, electrolyte, and efficiency the applications of fuel cells vary. Table 1.1 below summarizes different types of fuel cells along with their operating temperatures and applications.

Table 1.1 Types of fuel cells [9]

Type of Fuel cell	**Mobile ion**	**Operating temperature (^{o}F)**	**Applications**
Alkali	OH^-	300-400	Spacecrafts, zero-emission vehicles
Molten Carbonate	CO_3^{2-}	1200	Large stationary power plants, space heating, industrial processing or steam turbine
Phosphoric acid	H^+	300-400	Electric Vehicles, stationary power plants
PEM	H^+	175	Automotives, aircrafts, stationary power
Solid Oxide	O^{2-}	1800	Large stationary power plants, space heating, industrial processing or steam turbine

1.3 Nafion

An ionomer membrane is essentially a copolymer with a fluorocarbon backbone and repeating units of sulphonic acid or carboxylic acid end groups. The acid groups contain the mobile cations (positive charged H^+ ions) that are electro statically associated with fixed anionic charges on the polymer [10]. Since the fluorocarbon backbone is chemically and thermally very stable it is most suitable for thin membranes while the end acid groups are most appropriate for ion exchange. One such group of polymers that are modified to include sulphonic groups are most widely used in PEM fuel cells. DuPont de Nemours was the first to develop a perfluorosulphonic membrane which is commercially called Nafion® [10]. The backbone of Nafion® is polytetrafluoroethylene with regularly spaced perfluorovinyl ether pendant side chain and sulphonate ionic end group. The sulphonic ionic end group (SO_3M^+) contains the counter ion (H^-, Li^+, and Na^-) which can be partially or totally replaced by cationic groups or cations. This selectivity of cations versus anions helps the membrane to allow the passage of only cations and water, blocking the passage of anions even at high current densities and high ion concentrations resulting in high current efficiencies (> 98%). Also, the ionic exchange property provides the membrane with excellent ionic conductivity making it a better choice as a separator in chlor-alkali cells [10].

Thus, among the different ionomers Nafion® played a predominant role in the success of PEM fuel cells in transportation applications as it met the market needs by its excellent mechanical and thermal stability [3, 7]. GE's satellite program in 1996 (BIOS was a NASA space program that provided electricity and water for an animal orbiting in space in a satellite [2]) marked the beginning of the usage of Nafion membrane in fuel cells [4]. From then, there has been extensive research and development in the Nafion based fuel cell technology, especially in the transportation industry. Numerous vehicle prototypes have been manufactured and marketed globally to cater to the increasing demand of the automotive industry. The Mark 900 fuel cell stack developed by Ballard and DaimlerChrysler in late 1990's generated a total output of 75KW thus proving that PEM technology can meet the performance target of transportation applications [6]. All

major automobile companies throughout the world have demonstrated PEM technology in their fleet services and manufactured commercial fuel cell powered vehicles. A few of them are listed in Table 1.2.

Table 1.2 PEM fuel-cell based automotives [5]

Name of the Company	Vehicle Prototype	Fleet services
Toyota	FCHV-4	
Honda	FCX	
Nissan	X Trail	
Daimler Chrysler (Germany)		Hermes Delivery service
GM (Tokyo)		FedEx
GM (Washington DC)		US Postal Service
Hydrogenics		Purolator Courier Ltd.

High power efficiency, greater power density, quick start-up, faster response to changes in load compared to other electrolytes [6, 7]; simple, able to operate at a low temperatures, and zero emissions with hydrogen as the fuel made PEM fuel cells a viable technology for most transportation applications [5]. Foreseeing the competitiveness of the PEM fuel cell market, the US Department of Energy sponsored the Partnership for New Generation Vehicles Program (PNGV) program in 1993 with an aim to triple the fuel cell efficiency compared to current vehicles [6].

Despite the ongoing research and increasing number of PEM fuel cell vehicles there are still major problems that the industry needs to overcome in order to attain full commercialization. One of the major barriers that the industry is currently facing is the degradation of polymer electrolyte membrane in the fuel cell stack causing significant durability problems and thus increasing the cost of the cell. Despite the advantages of Nafion, the degradation and early failure of the membrane has been a potential barrier in the commercialization of PEM based fuel cells. The key reasons for failure are attributed

to operating conditions which induce mechanical, chemical and thermal stresses in the membrane reducing the proton conductivity, and mechanical strength considerably. In spite of very high longevities of per fluorinated ionomer membranes (60,000 hours at 80˚C in hydrogen fuel cells) the degradation and premature failure of the membrane has been a major barrier for fuel cell powered vehicles to become commercially viable [19]. In order to achieve a target of 5,000 operating hours of the PEM fuel cell stack for transportation applications, the durability of the membrane has to be greatly improved [4, 5 and 8]. The fuel cells in the automobiles are exposed to severe conditions such as inadequate humidification, reactant pressure; mechanical stresses etc leading to mechanical, chemical or electrochemical degradation of the membrane [3, 6 and 7]. In order to evaluate the performance of a fuel cell and predict its durability over the long term, it is important to understand the behavior of membrane under realistic operating conditions.

1.4 Degradation of Nafion

The chemical structure of Nafion® is composed of a fluorocarbon backbone with sulphonic acid end groups as shown in Figure 1.3. The sulphonic acid end groups are hydrophilic in nature while the fluorocarbon backbone chain is hydrophobic. Many conceptual models such as the ionic- cluster model, the polymer-aggregate model, the core-shell model, the bundle-cluster model, Eisenberg-Hird-Moore model have been developed to understand the interactions of the hydrophilic and the hydrophobic networks [11]. These models demonstrate that whenever there is a change in humidity due to water exposure or dehydration, the hydrophilic network absorbs water or contracts causing significant swelling and shrinking of the membrane. Though these models study chemical processes and transport phenomena they do not bridge the gap between transport phenomena and macroscopic property changes in the membrane during its operation and degradation in a fuel cell [11].

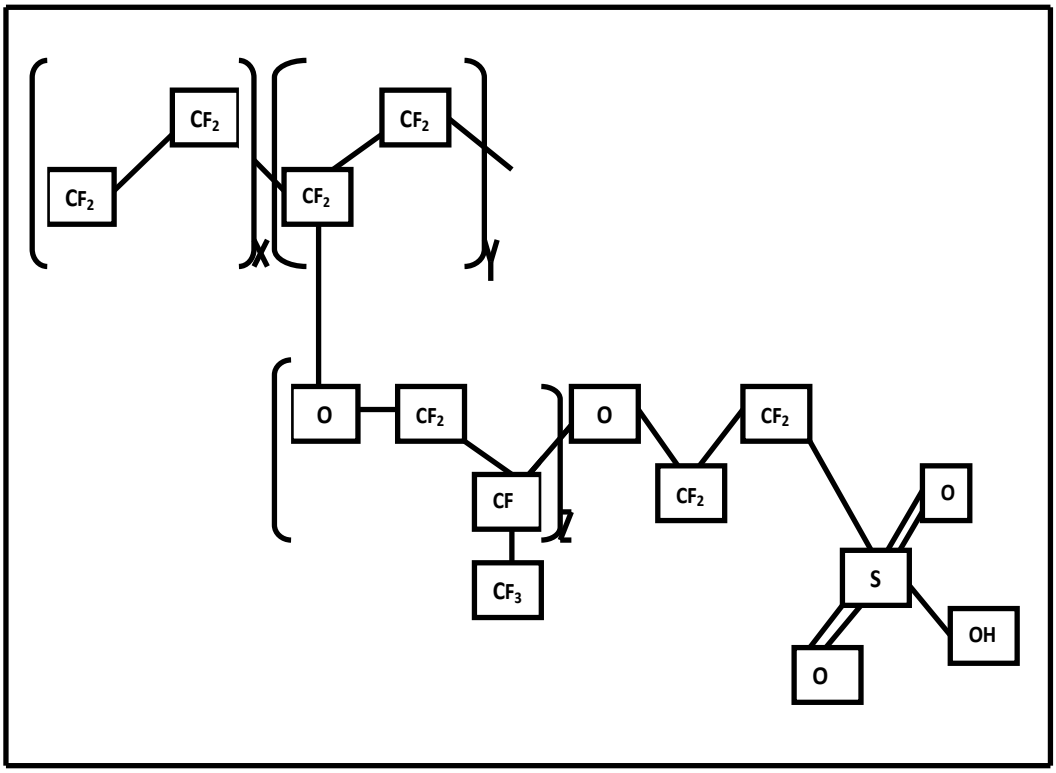

Figure 1.3 Structure of Nafion [10]

During the operation of a fuel cell, the membrane is exposed to reactant gases with varying temperatures and non-constant relative humidity's which cause the sulphonic acid end groups to swell and shrink over many times. The membrane is also constrained between the electrodes and bipolar plates inside the fuel cell which results in stresses forming in the membrane due to similar swelling and shrinking behavior. Also, the membrane is subjected to hygrothermal loading during its phase of fabrication in Membrane Electrode Assembly (MEA) (the membrane is mechanically constrained during the hot pressing of MEA and in a Direct Methanol Fuel Cell (DMFC) it is exposed to humidified hydrogen and air on both sides) [7, 8]. Rupture of the membrane occurs when a constrained membrane is subjected to RH and temperature cycling [3]. In a typical fuel cell powered automobile the membrane is exposed to frequent start-stop cycles, varying power conditions and non-ideal operating conditions which result in cyclic stresses and strains.

The swelling and shrinking behavior of the membrane can be explained by its chemical structure which is composed of hydrophobic and hydrophilic ionic groups that facilitate the transport of protons from anode to cathode. When the membrane is exposed to varying relative humidity's the hydrophilic ions segregate into nano-sized clusters [3]. These nano-clusters absorb water causing swelling of the membrane. When exposed to high temperatures or dry conditions these clusters shrink causing gradual shrinking and degradation of the membrane. This effect of hydration dynamics on the durability of the membrane was demonstrated by Kusoglu [14] and others. He showed that when a fuel cell is started the water content 'λ', defined as the number of water molecules compared to the number of sulfonic acid end-groups, on the cathode side of the membrane increased almost from 3 to 9. This high value of 'λ' corresponded to a swelling strain of 0.6 mm/mm in the membrane. Also, since the membrane was in a partially constrained condition it could not swell and hence developed very high hygral stresses (as high as 2-3 MPa) that were comparable to yield strength of the membrane. In addition, lack of water makes the membrane brittle and fragile [12] and the low humidification condition decomposes the crystal structure, decreasing ion channels and electrochemical conductivity [8]. An X-ray Diffraction study of Nafion® revealed that the characteristic peak (18° diffraction angle) is greatly decreased due to low humidification.

Thus the perfluorosulfonate acid proton exchange membrane is subjected to mechanical and hygro-thermal loading throughout its life right from its fabrication phase to its usage in a fuel cell. Hence it is important to understand the transient behavior of the membrane along with the steady state in order to model the fuel cell performance subjected to realistic operating conditions.

1.5 Previous Work

Numerous studies have been conducted on the mechanical and electrochemical degradation mechanisms in the fuel cell membranes. Ahmet Kusoglu and A.M. Karlsson studied the mechanical response of a fuel cell membrane electrode assembly subjected to

a single hygro-thermal cycle [14]. They found that compressive, plastic deformation of the membrane which occurred due to loading also led to tensile residual stresses after unloading. The formation of cracks and pinholes in the membrane may be accounted to the residual in-plane stresses. Haolin Tang and Shen Peikang studied the electrochemical characteristics of the MEA assembly together with the mechanical breach of constrained Nafion due to relative humidity and temperature cycling [15].They found that the fatigue limit of the constrained membrane was less than or equal to 1.5 MPa which is $1/10^{th}$ of the tensile strength of the membrane. The shrinkage stress and dimensional change for RH cycling (from water soaked state to 25% RH state) were as high as 2.23 MPa (higher than the fatigue limit) and 11% respectively. While the shrinkage stress induced by temperature cycling was much less (0.14 MPa) indicating that the shrinkage stress induced by RH cycling leads to mechanical breach and subsequent failure of Nafion PEMs. In the electrochemical study of MEA, they found that the degradation of membrane results from H_2O_2 attack formed at a potential close to H_2 adsorption potential [7]. The gas diffusion media used in proton exchange fuel cells tend to possess very high inhomogeneous microstructures as they are produced by conventional paper manufacturing processes. This may result in localized over compression of membrane material due to non uniform thickness along with compressibility of GDM. Yongqiang Li conducted a novel experimental test to measure the compressibility of GDM. The testing method revealed that a compressive stress as large as 2.30 MPa in various hot spots (of order 100s μm to 1mm in size) of membrane were caused due to a nominal plate compression of 0.68 MPa [13].

Many researchers have modeled the electrochemical and mechanical response of the PFSA membrane in the past few years. Haolin Tang and Shen Peikang studied the mechanical properties of a constrained Nafion in an environmental chamber on a universal test machine with independent T/RH control [7]. Roham Solasi and Yue Zou also investigated the mechanical behavior of constrained PEM fuel cell membrane subjected to hydration and temperature cycles [3]. The membrane was constrained to replicate the clamped membrane condition in the fuel cell in an environmental gas

chamber with independent RH/T control. The stress- strain behavior and the expansion/ contraction of constrained membrane due to changes in relative humidity and temperature were measured. Again, Haolin Tang and Shen Peikang along with Fang Wang, San Ping Jiang and others studied the electrochemical characteristics of MEA assembly together with the mechanical breach of constrained Nafion due to RH/T cycling [7]. In the electrochemical study the membrane was sandwiched between two platinum electrodes to form an in-house fabricated membrane-electrode-assembly. The proton conductivity of the membrane was the measured using impedance analyzer under the conditions of 100% relative humidity and 60˚C. Other researchers like C.Gavach and G. Pamboutzoglou investigated the kinetics of ion transport in Nafion® perfluorosulfonic acid membrane using the AC impedance technique [16]. The conductivity of pre-treated membranes was measured at regular intervals after being hydrated initially and then vacuum-dried. The membrane resistance was measured from the intercept of impedance diagram with the real axis.

Liu et al. was the first to study both the electrochemical and mechanical properties independently [11]. While he measured the conductivity changes in the membrane when being held at constant strain and submerged in water and stress relaxation was measured separately in air at various temperatures. He found that when the membrane was stretched the proton conductivity increased in the direction of strain. It increased greatly with a rise in temperature and decreased exponentially with time when the temperature was decreased. The stresses of membrane in both atmospheric and de-ionized condition were found to decay more quickly compared to the proton conductivity [15]. Although Liu et al. conducted independent tests to show stress relaxation and conductivity varied due to straining of the membrane, he did not measure the conductivity when the membrane was actually strained in air. Also, the electrochemical and mechanical response of the membrane while it is being strained in air would greatly depend on the water content in the membrane.

Most of these studies showed the steady state response of the membrane subjected to mechanical and hygro-thermal loading. It is important to model the transient response along with the steady state as the membrane is subjected to mechanical and electrochemical degradation simultaneously. The in-situ measurement of mechanical and electrochemical properties can be used in the development of better fabrication processes and membrane materials.

1.6 Objectives

The objective of this research project is to measure the changes in conductivity of the membrane due to mechanical and electrochemical loading. A custom environmental chamber and a conductivity measurement test cell were built to accomplish this objective. The membrane was stretched to a specific strain and through plane impedance at different time lapses before and after stretching was measured. The relative humidity and temperature were varied along with imposing the mechanical constraints. The test set up would allow measurement of changes in the impedance of the membrane inside the chamber environment without exposing the membrane to non-test environmental conditions such as stress relaxation due unloading of membrane and varying relative humidity and temperature conditions.

The difficulty in measuring the changes in stress, relative humidity and temperature while the membrane is being transferred from the test machine to electrochemical impedance spectrometer has been overcome using the facility described in this thesis. The data obtained can be used to accurately model the interdependence of mechanical and electrochemical properties in the membrane. Also, the time dependent changes in the mechanical and electrochemical properties of the membrane due to stress and hygro-thermal loading can further be used to develop better MEA fabrication processes and membrane materials.

1.7 About the Thesis

This thesis is divided into three sections:

- The first section discusses the design and working of a novel experimental facility that allows the continuous measurement of stress and impedance due to changes in relative humidity and temperature
- The next section discusses the experimental procedures and data collection
- The final sections present a visco-elastic stress relaxation model for a specified strain rate, relative humidity and temperature.

2. PROCEDURES

2.1 Test to Find the Water Content of the Membrane

DuPont™ Nafion®PFSA resins produced by the copolymerization of tetrafluoroethylene and alkyl vinyl ether with sulphonyl acid fluoride are per fluorinated precursor resins in sulphonyl fluoride ($-SO_2F$) form [22 and 30]. In this form, the polymer is a thermoplastic and is not chemically active since it lacks the cation-exchange properties as compared to other Nafion® PFSA products. The membrane material is chemically treated in order to make it usable in cation-exchange applications. The hydrolyzed resin is converted into acid form ($-SO_3H$ or H^+) by a chemical treatment [30]. After being chemically activated from the salt form to acid form, it reacts more aggressively with its surroundings. It absorbs and exchanges moisture with its surrounding environment [17]. Hence, it is important to study the water uptake (λ) of Nafion ® as the conductivity of membrane is related to water content [15].

Commercial Nafion® (packaged at 23°C and 50%RH) will equilibrate with the ambient relative humidity conditions when it is unpacked [22]. It is important to know the extent to which the membrane equilibrates with the ambient conditions of the chamber so that the effect of any further changes in relative humidity and temperature inside the chamber on the stabilized membrane can be studied effectively. If the membrane is not allowed to equilibrate with chambers environment, the water uptake condition of the membrane can affect the impedance of the membrane subjected to any mechanical/hygro-thermal loading.

Also, knowing the exact water content in membrane will allow a better estimate of 'λ' for every experiment. It is also necessary to find the time taken by the membrane to

equalize with chambers environment since it gives an estimate of the wait time needed before subjecting the membrane to any loading condition. To evaluate the water uptake performance and estimate time taken by Nafion® for equilibration two tests were performed on two different membrane sets. Each membrane set comprised of three specimens of 20mm wide and 60mm long which were cut out from a commercial Nafion 115 sheet using a steel rule die in machine direction or perpendicular to machine direction [11]. The membrane was placed between upper and lower half of the steel rule die which was in turn placed between the stationary and moving arm of a press. If the long side of the die was placed parallel to direction of the grain in the Nafion then it is referred to as machine direction and vice-versa. Both directions produced similar sized samples. The weights of membrane in each of these sets were noted before and after every test.

- For the first test 400ml of 0.5M H_2SO_4 was prepared by adding 10.66 ml (400 X 0.5 X 0.0533) of H_2SO_4 into 389.34 ml of DI water. The first membrane set was boiled in 0.5molar sulphuric acid for one hour and later boiled in de-ionized water for another one hour
- In the second test, the membrane set was not subjected to any chemical treatment. The membrane set comprised of three as received specimens at ambient conditions

The two membrane sets obtained from the above two tests were preserved in closed glass vials. The cap of the glass vials was opened by unscrewing them and the open mouth glass vials were placed in a chamber which had a provision for purging water vapor saturated N_2 gas. After the two specimens glass vial sets were placed in the chamber humidified N_2 gas was purged into the environment (the method of passing humidified N_2 gas using a humidifier is described in detail in Section 2.5). The weights of glass vials were recorded at regular time intervals using an Analytical balance (manufactured by Mettler Toledo, model number PG503-S, and of precision 0.001 grams). Each time, the weight of membrane in the glass vial was calculated by deducting the weight of glass vial from weight of glass vial together with the membrane. After

recording the final weight, the percentage of water content was calculated by finding the difference in weights (change in wt. /original wt x 100).

2.2 Material Test System and Controller

The material test system used in this experiment was an MTS 810 Universal testing machine. The main components of the system include a floor-standing base, hydraulically powered crosshead positioning, a 100 lbf load cell, fixtures and grips, hydraulic power unit with a heat exchanger and a 458.12 controller. Figure 2.1 highlights the main components of the MTS used in this experimental setup. Figure 2.2 shows the grips, membrane, heater and a RH meter which are located inside the chamber.

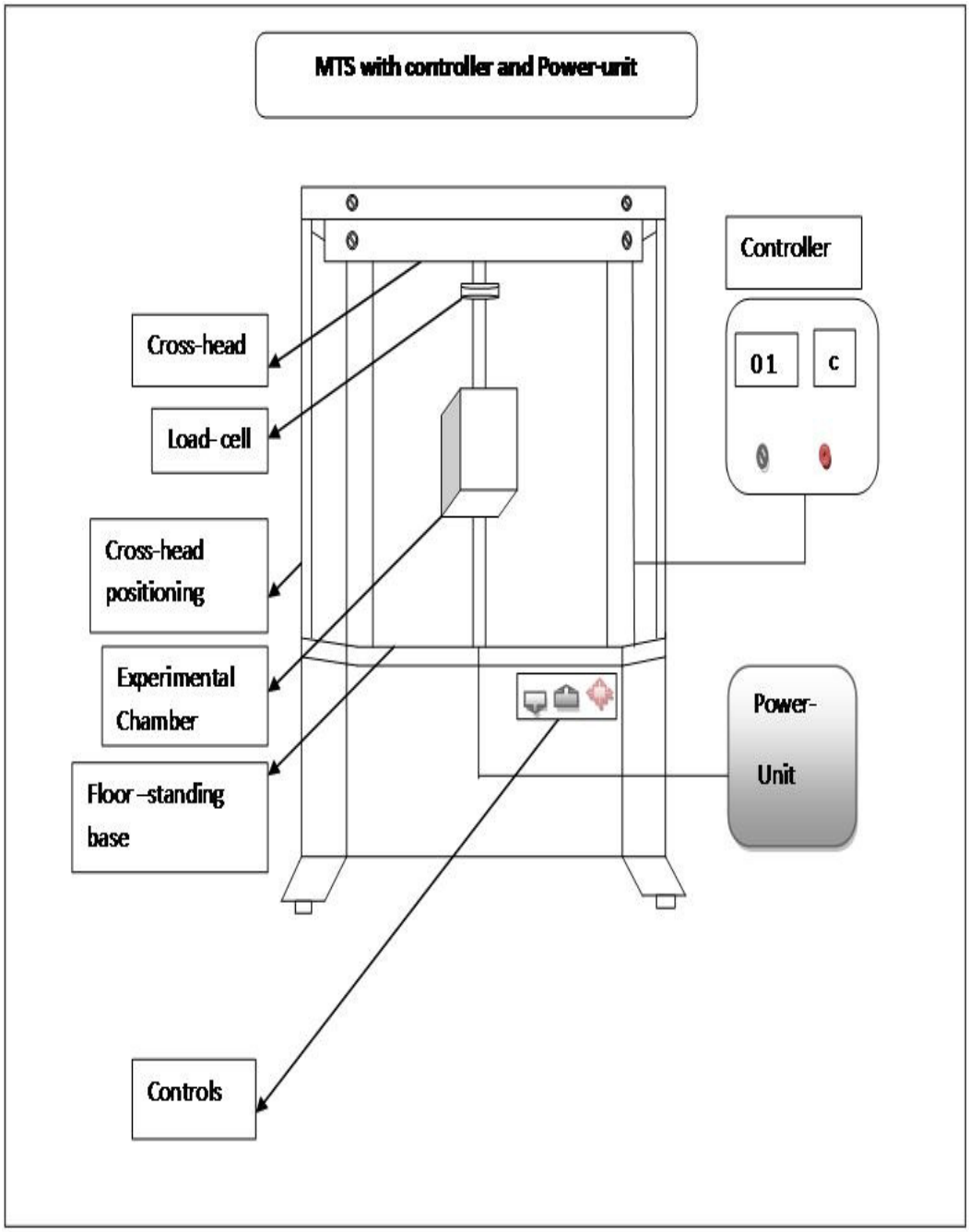

Figure 2.1 Material Test System and Controller

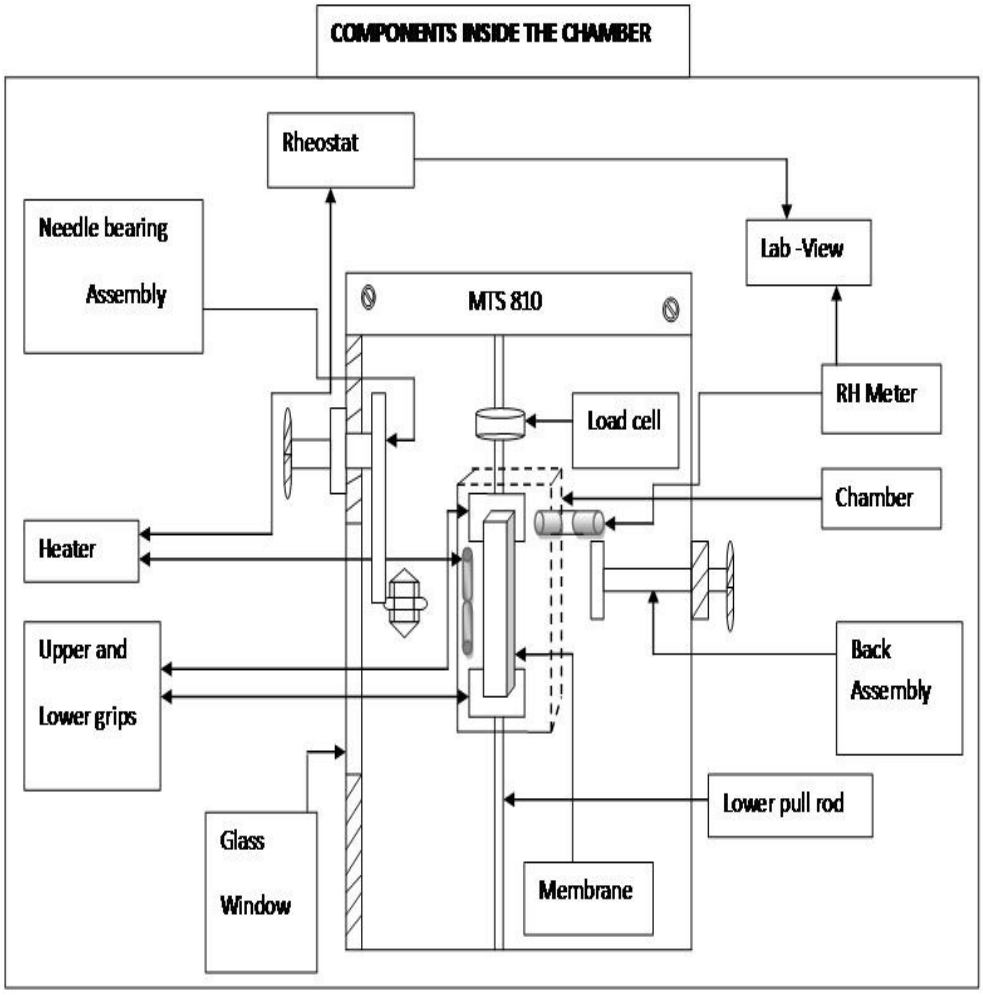

Figure 2.2 Components inside the chamber

The experimental chamber was a custom-made humidity and temperature chamber of 14cm in width and 23cm in length. The front side of the chamber had a detachable glass window in the center and therefore the changes occurring in the membrane were visible from outside of the chamber. The other three sides had provisions for RH meter, input N_2 gas tube, Potentiostat cables, wires from the heater, thermocouples, needle bearing guide sets and micrometers which were a part of the conductivity measurement test cell. The upper and lower faces of the chamber had bores in the center for the rods that are used to hold to upper and lower parallel plate grips. The rod holding the upper grip was attached to a load cell and was used to measure the load changes in the membrane. The tubular heater was installed inside on the back wall of

chamber and the wires coming out of the heater were connected to a rheostat and lab-view signal. The RH meter was a thin film polymer capacitor with a 20 second response time that could be inserted or removed in to the side wall of the chamber.

Installation of the membrane was accomplished as the following process: the lower grip was unscrewed and one end of the membrane was fixed between the parallel plates of the grip (the grips could be unscrewed and screwed back as the pull rods and grips had threaded bores). After fixing the membrane, the lower grip was screwed back to the lower pull rod after which the other end of the membrane was fixed between the parallel plates of the upper grip.

The chamber is attached to the lower pull rod which is actuated by the MTS. The upper grip is attached to the load cell which is fixed to the stationary upper brace. Therefore the chamber and lower grip move with the lower pull-rod while the upper grip stays in a fixed location. The moving of the chamber with the lower grip helps to keep the instrument in position with the membrane. The maximum distance that the lower grip can move is determined through the controller using a range cartridge. The range used in these experiments was +/- 20mm. The definition of the physical location of the zero point, the point where the displacement transducer reads zero, is arbitrarily set to accommodate the chamber. The maximum displacement from below zero to above zero is termed as Full Scale (FS) (lower and upper FS are shown in Figure 2.3). The displacement and the speed of grip movement are programmed in terms of FS. A typical displacement control program used in these experiments induces a 7% (2mm) strain in the specimen at a rate of 50%FS. The rate is the percent full scale per second and the end level is the desired displacement from the zero point either positive or negative.

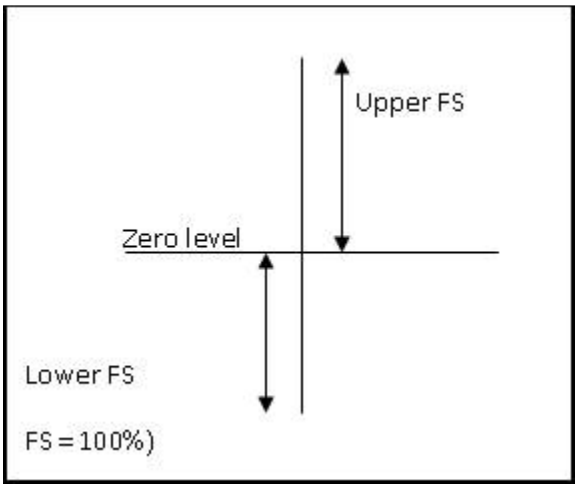

Figure 2.3 Full Scale and Zero level of lower grip

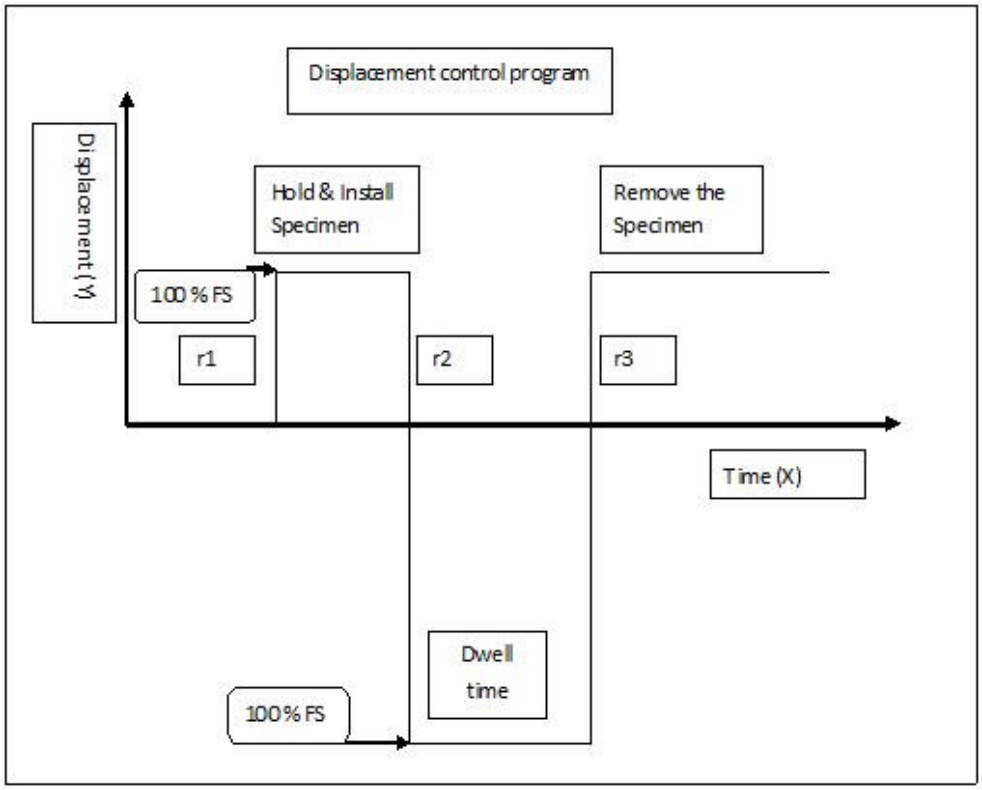

Figure 2.4 Non-linear displacement control program

Figure 2.4 illustrates the stress relaxation procedure that was programmed into the MTS 458.12 controller. The lower grip was moved to a set point (a positive value) initially and at this point the specimen was installed. After the specimen was installed it was stretched to the next end point at a specific rate r2 (mm/sec). The specimen was allowed to stress relax a pre-determined amount of time (dwell time). After the completion of experiment the lower grip was moved back to the original position using the 'return to zero' command. The stretched specimen was removed from the grips before turning off the machine.

2.3 Conductivity Measurement Test Cell – Design & Working

A conductivity measurement test cell is a device that measures electrochemical impedance by the application of a small AC current. The electrochemical impedance (which is the ability of a circuit to resist the flow of electrical current) of the membrane is measured by applying a small sinusoidal voltage to the cell and then measuring the response which is AC current over a specified frequency range.

A custom made test cell was developed to test the impedance of the membrane while it is being stretched inside the environmental chamber. Since the test cell was incorporated inside the chamber, impedance measurements could be made during the process of the experiment and the possible changes that can occur to the membrane conductivity while it is being transported from experimental setup to impedance testing equipment have been prevented. The changes in conductivity may occur due to different environmental conditions or storage between stations.

The test cell could be moved out of view of the chambers glass window when not in use facilitating for additional measurement techniques such as optical or laser extensometry [11] (the chamber has a detachable glass window by which the changes in the membrane could be viewed from outside of the chamber).

The conductivity measurement device consisted of two assemblies that came in contact with the membrane specimen from either side (3D model of test cell inside the experimental chamber is shown in Figure 2.5).

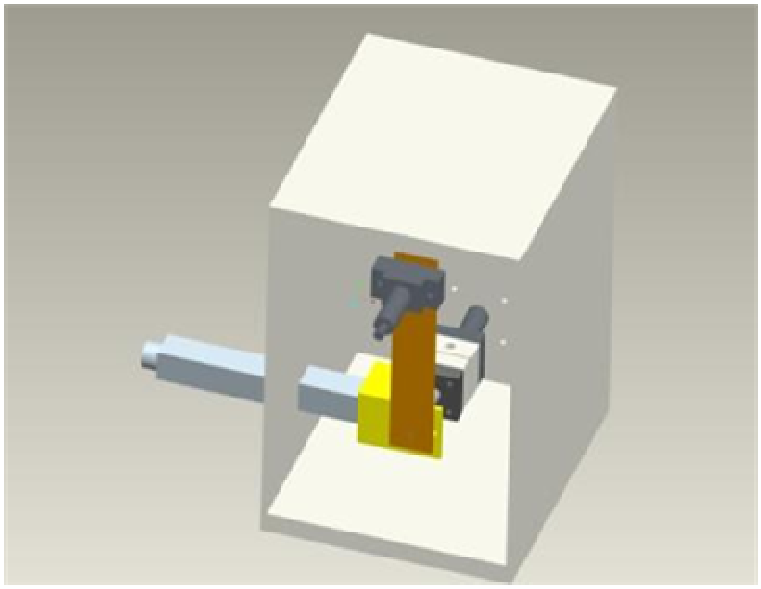

Figure 2.5 3D model of conductivity measurement test cell incorporated inside the chamber

The front assembly is comprised of Teflon probe, steel block, L-block made out of steel, needle bearing guide set, a vertical plate, linear moving micrometer and a micrometer mount. The back assembly is comprised of a Teflon probe, steel block, and linear moving micrometer and a micrometer mount. Two different views of the assemblies are shown in Figure 2.6.

During an impedance test, the electrodes mounted on the Teflon probes of the test cell come in contact with the membrane from either ends. On the front side of one Teflon probe, there were two platinum wires that ran parallel to each other. The other Teflon probe that comes in contact has two palladium foils that also run in a parallel fashion at 180 degrees to direction of platinum wires. Through plane impedance of the membrane was measured by connecting the input cables from a Gamry Potentiostat to the wires running out from the platinum wires and palladium foils of the Teflon probes. The Gamry

software was used to measure the current at various frequency points for the applied voltage. Impedance tests were conducted before and after stretching and during the stress relaxation phase of the membrane. With the help of micrometers and needle bearing guide sets, the Teflon probes were brought in and out of contact with the membrane after each impedance test so that the membrane is not artificially constrained during stretching or stress relaxation phases.

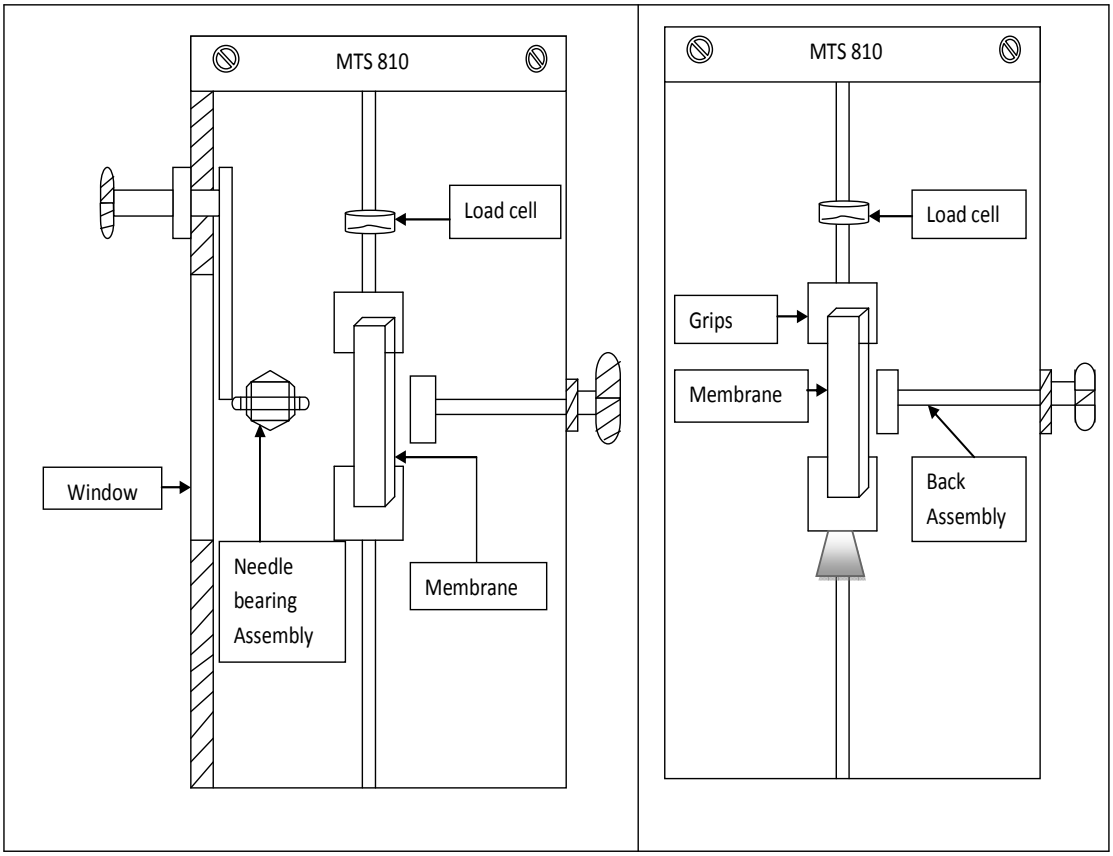

Figure 2.6 Two different views of conductivity measurement test cell

The conductivity measurement test cell was operated by moving the front and back assemblies. The movement of the two micrometers brought the two Teflon probes in contact with the membrane and with the aid of these linear moving micrometers; the assemblies could be retracted back. Thus the two micrometers controlled the movement of the assemblies bringing them gently in contact with the membrane in a transverse

direction (Figure 2.6). These micrometers were aligned in linear fashion and the thimble of the micrometer heads were locked after the electrodes came in contact with the membrane specimen ensuring precise positioning of the electrodes and removal of additional pressure/lateral loading on the membrane. The thimble of micrometers was turned until they were clicked to ensure that the electrodes apply the same pressure on the membrane during every experiment. The needle bearing guides provide the front assembly with two degrees of freedom so that the assembly could be retracted out of the view of the window for subsequent testing. The movement of the back assembly was rather simple with the micrometer providing it with only the transverse motion.

As the experimental chamber was a custom made size steel box, dimensions of different parts of the front and back assemblies had to be consistent with the chamber. The dimensions were chosen such that the assemblies would fit inside the chamber without colliding with its walls. The Teflon probes should come in contact with the membrane during the impedance test and must be withdrawn after the completion of the test to prevent constraining the membrane during stretching or stress relaxation phases. Hence the assemblies were designed to allow motion thus providing degrees of freedom: the front assembly was designed to incorporate an L-shape structure allowing movement in longitudinal and transverse directions while the back assembly was designed to move in transverse direction alone (transverse direction is defined as the movement of the Teflon probes towards the front or back walls of the chamber and the longitudinal direction is their motion towards the side walls).

2.4 Gamry Potentiostat

The electrochemical impedance of the membrane was measured using a Gamry Reference 600 Potentiostat. Gamry EIS is a reliable method that can be used to measure the impedance in a wide range of frequencies between 1mΩ to 10^{13}Ω [24]. The Reference 600 instrument is a research grade electrochemical instrument that can be used as a Potentiostat, Galvanostat or a Zero Resistance Ammeters (ZRA) [25]. A Reference 600

Potentiostat requires a computer for its use and was connected to the computer using a USB connection. Reference 600 software has been installed as a part of Gamry framework in a Microsoft Windows ™ compatible computer. The system can be used in Potentiostatic, Galvanostatic, and Hybrid EIS modes to measure the impedance of the specimen between specified frequency range. Figure 2.7 shows the connections between the specimen, Gamry Potentiostat and the computer.

The Gamry Potentiostat had four input cables from which two were connected to the wires that ran out from the palladium foils while the other two were connected to the platinum wires that come out from the test cell. Before the first impedance measurement, the Potentiostat was calibrated with the universal dummy cell. From the different modes available, the conductivity measurement test cell and the Potentiostat were connected in the "Membrane Electrode Connections (MEC)" mode since this separates the two electrolytes (a reference and counter electrode). In the MEC mode, each of the two counter electrodes (green, red) and the two reference electrodes (blue, white) were connected to the platinum wires and palladium foils. The ground (black) was connected to ground while the counter sense (orange) cable was left open.

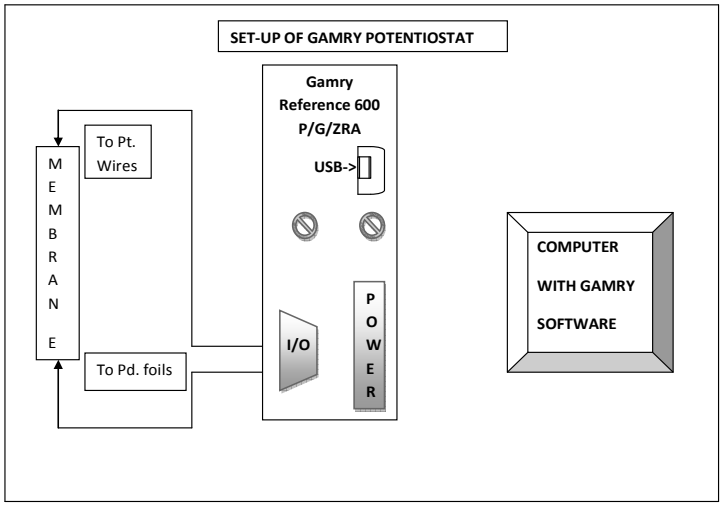

Figure 2.7 Connections between Gamry Potentiostat, computer terminal and test specimen

The Gamry Potentiostat could employ three methods to measure the through plane impedance of the membrane. In a Potentiostatic EIS method, the impedance was measured by applying a sinusoidal voltage to the electrodes and then measuring the current through the membrane. While the Galvanostatic EIS and Hybrid EIS applied AC current and then measured the potential between the electrodes. In the Hybrid EIS, the first measurement was made using the user-specified initial potential and then the impedance at all other frequencies was performed in Galvanostatic mode using the current measured at the initial frequency. While both the Potentiostatic and the Hybrid EIS could be employed to measure the impedance of a hydrated membrane, hybrid mode could not be employed to measure the impedance of a dry membrane. The reason for this is the dry membrane has a high resistance, and the application of the small AC current supplied by the Gamry Potentiostat would result in zero or nearly negligible voltage between the reference electrodes. Therefore, a Potentiostatic EIS technique which applies voltage to measure the impedance was employed. By using a Potentiostatic EIS technique, the impedance of both hydrated and dry membrane could be measured.

The procedure to perform an impedance measurement is as follows. The frequency range was set between 100,000 Hz to 0.1 Hz and the input AC voltage was set as 10 milli volts and an input area of 2.5 cm^2. The DC amplitude versus the reference electrode was set to zero since there was no reference electrode in the membrane electrode connections mode. The results, which were stored in a .DTA file, could be extracted and analyzed using statistical tools such as Excel. The results could also be analyzed in the Z-view Echem Analyst software which is a part of the Gamry software framework. A typical Potentiostatic interface consisted of the following input parameters:
Frequency Range = (100,000-0.1) Hz;
AC Voltage (mV rms) = 10;
DC Voltage (V) = 0 vs. E_{ref};
Area = 2.5 cm^2

2.5 Temperature and Relative Humidity Apparatus

The temperature and the relative humidity (T and RH) were controlled in the chamber through a gas purge and heater system. The temperature control apparatus consisted of a tubular heater, solid state relay, customized lab-view program, rheostat, multi-meter, thermo couple and thin-film polymer capacitor as shown in Figure 2.8. The temperature of the environment was controlled by turning on and off the tubular heater inside the chamber. The heater was controlled by a signal generated by lab-view. The output of lab-view was connected to a Solid State Relay (SSR) which then switched on and off the heater. The rate of increase or decrease in temperature due to the tubular heater was changed by adjusting the voltage supplied to the heater. This was accomplished by manually controlling the rheostat connected between the heater and the SSR. The input and output voltage of the rheostat was checked using a multi-meter and accordingly the voltage was adjusted to reach the target temperature. The temperature inside the chamber was measured using multiple thermocouples. The temperature was recorded in lab-view.

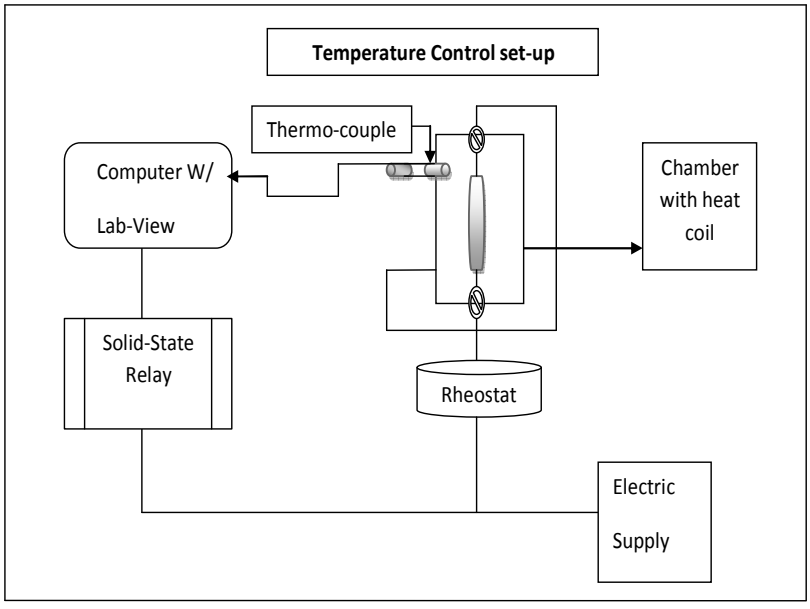

Figure 2.8 Temperature control set-up

The components of the RH control system include two N_2 gas tanks, a humidifier, a hot plate, two pin valves, a flow-meter, and a thin-film polymer capacitor based relative humidity sensor as shown in Figure 2.9. The relative humidity inside the chamber was controlled by circulating a mixture of dry and water-vapor saturated gas. The RH sensor was connected to lab-view which read and recorded the relative humidity inside the chamber over the duration of the experiment. The RH sensor was calibrated using 7% NaCl and 11% $MgCl_2$ salt solution at ambient conditions to ensure that it records consistent relative humidity values. The N_2 gas was supplied from two tanks that had two pressure regulators which were used to control the output pressure (0-4800) psi from the cylinder to the input pressure (0-30) psi of the flow-meter. The flow meter was adjusted to circulate the gas to the humidifier (which was essentially a pressure vessel filled with DI water, copper tubing was coiled and attached to the gas inlet) and chamber at a constant rate (approx. 1-2 psi or 80-90 ccm). The humidifier was filled with de-ionized water and was placed on a hot plate which was used to increase the temperature of the DI water inside it. The Nylon tubes from the humidifier and the second N_2 tank were combined in to a single outlet using a two-pin valve which had a dial of range (0-10) which was uses to control the output flow of the gas.

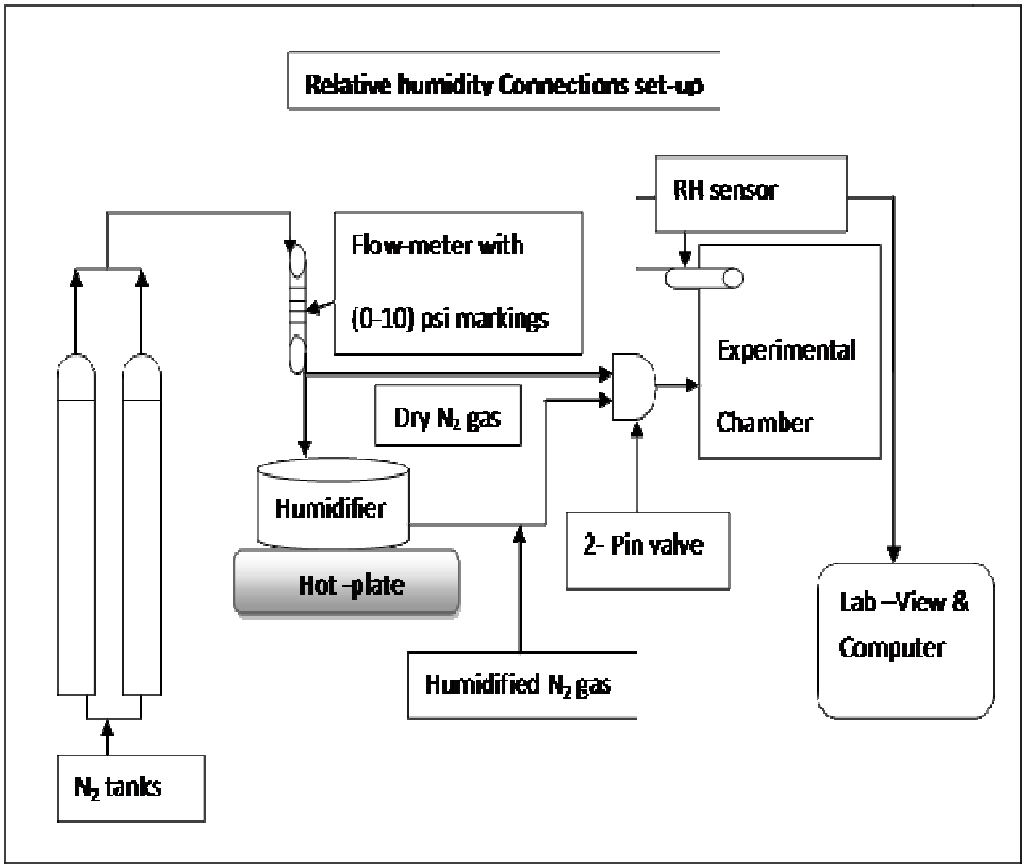

Figure 2.9 Relative humidity control set up

2.6 Lab-View

A custom lab-view program was used to record the changes in relative humidity, temperature, displacement and load. The front panel of the lab-view user interface as shown in Figure 2.10. The lab-view program had a provision to record the raw as well the calibrated data. The raw data was the data that was recorded directly from the MTS machine and the various input signals while the calibrated data was the data that was recorded after the calibration parameters were applied to the input signals. The calibration parameters that were incorporated in the block diagram linked the input and output parameters of the program. The calibration parameters are the values obtained after calibration of temperature and RH sensor at ambient conditions. In the first step, after displaying the displacement, force, temperature and relative humidity (both raw and

calibrated data can be displayed by clicking their respective display buttons), the target temperature was set. The temperature inside the chamber was controlled by a simple Boolean operation. The current temperature in the chamber was compared to the set point temperature and the heater was cycled on or off to change the temperature.

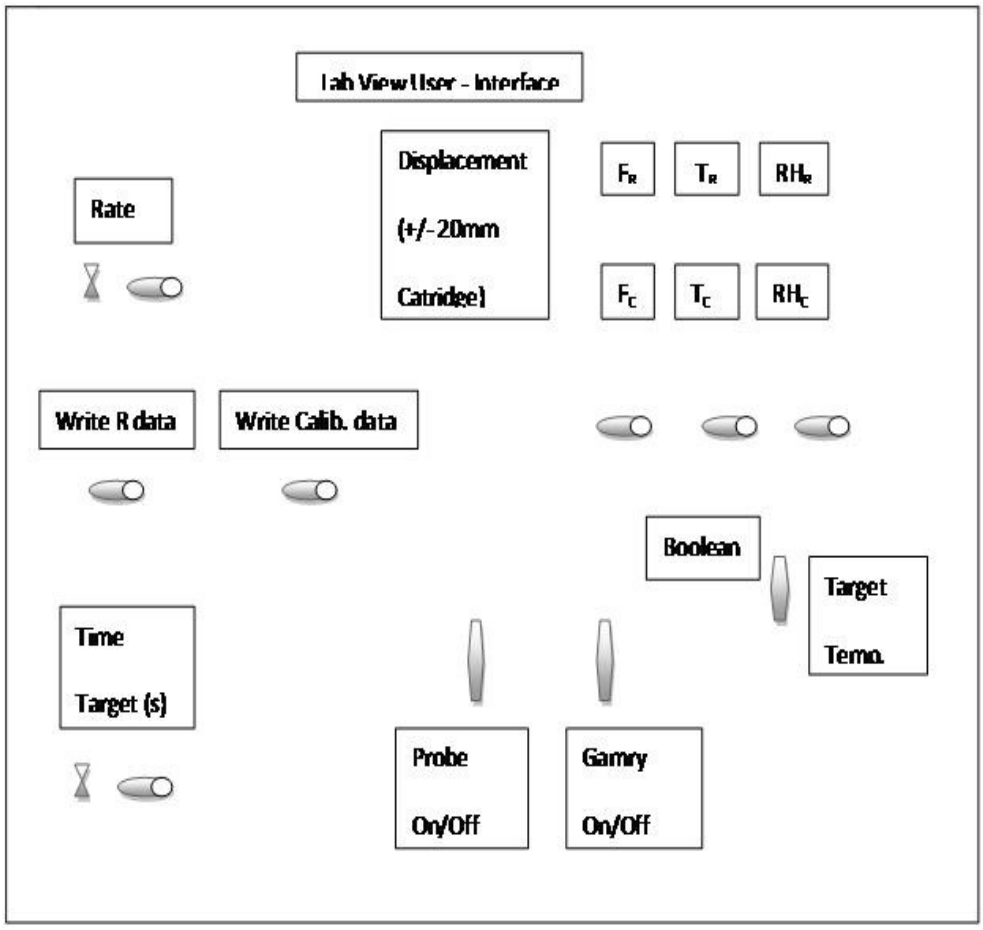

Figure 2.10 Displacement control lab-view user interface

The relative humidity inside the chamber was manually controlled by circulating a mixture of dry and humidified N_2 gas from the two N_2 tanks and the value of relative humidity was recorded in lab-view. The increase/decrease in temperature inside the chamber was also recorded in lab-view while it was controlled using a heater and Boolean operation that worked according to a set temperature. The recording of load data was started after membrane installation. This was done to ensure that any pre-load

(though a negligible value) during the installation of the membrane does not get added to the actual load on the membrane. After the membrane was installed between the grips the displacement was changed until the load was zero. Subsequent changes in load due to stretching and stress relaxation were then recorded. The membrane was stretched by running the controller program fed in to the controller before the membrane installation. Similarly the displacement was recorded after the membrane was installed between the grips. The movement of lower pull rod before the installation process was not recorded. After the membrane installation, the controller program was run which stretched the membrane and moved the lower pull rod further down to a level specified in the program. The membrane was left at this position during the remaining stress relaxation phases and the constant displacement values were recorded in lab-view. The recording of the data in lab-view was stopped immediately after the completion of the experiment and the changes in load/displacement during the de-installation of the membrane from the MTS were further not recorded.

During an impedance test, the probes of the conductivity measurement test cell came in contact with the membrane and were retracted away after the completion of the test and hence the front panel had a provision to record the time point at which the probes come in contact and the time point at which the impedance test was started. This helped to keep a track of the data points that may have caused a disturbance in load and the time points during the stress relaxation when the impedance was measured. Two additional Boolean switches were used to accomplish this purpose. The rate (number of data points per second) and time target boxes (time lapse between two data points) were used to control the rate and time lapses between data points.

2.7 Methodology, Connections and Data Collection

The current experimental facility allows continuous measurement of load, displacement, temperature, and relative humidity while allowing periodic measurement of impedance of the membrane while subjecting the membrane to changes in relative

humidity, temperature and load. The complete set of connections for the experimental facility is shown in Figure 2.11.

First, the specimen was cut from the Nafion® 115 sheets (the direction and the method for cutting are described in detail in Section 2.1) into 20mm X 60mm size specimens in the machine direction (MD) or transverse to the machine direction using a custom made steel die. The same die was used for each experiment and the same direction was chosen to get consistent results. The specimens were later subjected to pre-treatment to acidify the specimen and the method consisted of boiling the specimens in 0.5M H_2SO_4 for 1 hour followed by boiling it in DI water for 1 hour. The acidified specimens were stored in DI water at room temperature before they were used for the experiments. The specimen was mounted between two parallel plate grips in the chamber. The specimen was allowed to equilibrate with the test conditions before it was subjected to testing.

The conductivity measurement test cell was incorporated inside the chamber to measure the impedance of the specimen. In the absence of an impedance spectrometry device that is incorporated into the mechanical testing device, the membrane needs to be transferred from the MTS to an impedance testing station. During its transfer, the changes in the humidity and temperature are lost. Also when the membrane held at constant strain, is exposed to ambient conditions during its transfer the stress in it may vary significantly due to the effect of factors like stress relaxation or loading/unloading conditions.

The relative humidity of the test environment was controlled by circulating a mixture of dry and saturated vapor gas for which two N_2 cylinders, flow-meter, and humidifier were connected in series. The temperature was controlled using a heater installed inside the chamber. The membrane was strained at a constant displacement rate. The values of load, temperature and relative humidity were recorded using the lab-view program.

The impedance of the membrane specimen was measured before, after and during stress relaxation using a Gamry Potentiostat connected to the conductivity measurement test cell. The Gamry Potentiostat employed Potentiostatic EIS technique which measured the impedance of the membrane by applying a sinusoidal voltage and then measuring the current between the electrodes. The impedance was measured by applying a small AC voltage signal (10 milli volts) between the frequency ranges of 100,000 Hz to 0.1 Hz. The membrane resistance was obtained by extrapolating the Nyquist plot on the high frequency side on to the real axis [11]. Thus the current experimental facility allowed the continuous measurement of mechanical properties and periodic measurement of impedance in the specimen due to changes in load, temperature and relative humidity.

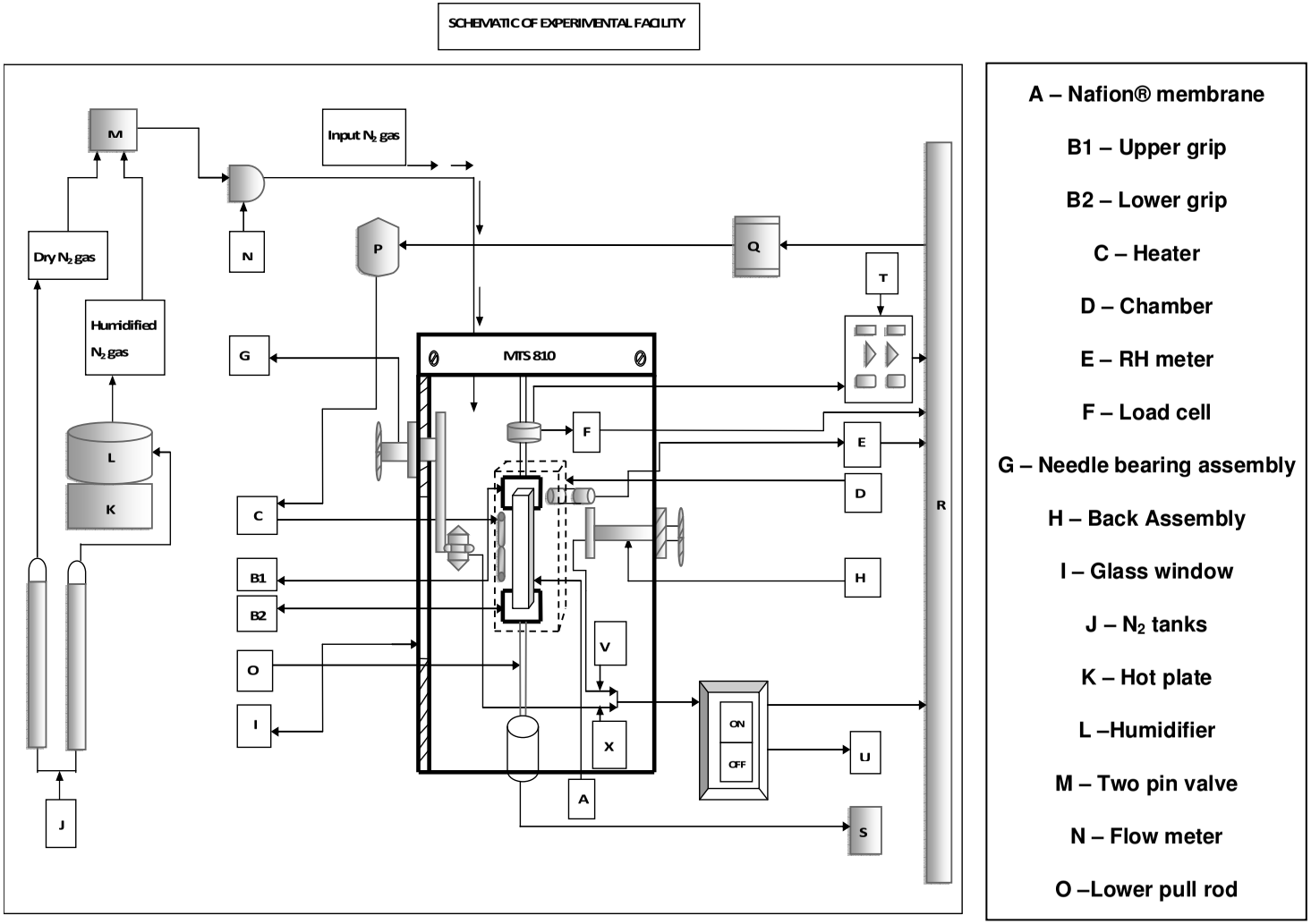

Figure 2.11 Schematic of experimental facility

2.8 Experiments and EIS Techniques

The experiments that were conducted to model the interdependence of mechanical and electrochemical properties of the membrane at a fixed strain rate were:

- Stress relaxation at ambient conditions
- Stress relaxation with temperature control (30˚C, 60˚C and 90˚C)
- Stress relaxation with relative humidity cycling with two different dwell times (20 min and 10min).

For all three sets of experiments, through plane impedance measurements were made before stretch, after stretch and at different time periods during stress relaxation phase of the specimen.

The impedance measurements for the above sets of experiments were conducted in two different modes as listed below:

- Experiments at ambient conditions - both Galvanostatic and Potentiostatic modes
- For temperature control and RH control experiments - Potentiostatic mode only.

2.9 Stresses in the Membrane

The integrity of Nafion® is greatly reduced due to the formation of pinholes and cracks which may be caused by the development of different stresses in the membrane during its fabrication in the Membrane-Electrode-Assembly (MEA) as well as during its usage in fuel cells. During the operation of a fuel cell, the electrolyte membrane in the fuel cell is subjected to cyclic hydration due to frequent start, shut-down and changing power requirement of the vehicle. The hydration and dehydration of the membrane cause mechanical stresses in the membrane [28]. The operation cycles also result in mechanical fatigue of the membrane electrode assembly and further mechanical degradation of the membrane [28 and 29].

When the membrane is stretched and held at a constant strain it creates tensile stresses in the membrane. The changes in humidity and temperature inside the chamber induce thermal expansion/contraction and swelling/shrinking which result in mechanical stresses in the constrained membrane. These mechanical stresses in the membrane replicate the stresses the membrane that can be generated due to RH cycling during the operation of a fuel cell. The stress relaxation behavior of membrane along with the conductivity changes during the experiment while the membrane is subjected to hygro-thermal loading replicates the condition of membrane subjected to realistic operating conditions.

The specimen was stretched to a strain of 7% and was held constant at that displacement. After the application of 7% strain, the specimen entered the stress relaxation phase as the applied displacement was held constant at this point. Therefore the force applied varied as the stress decayed over time due to stress relaxation of the membrane. Thus the stress in the membrane before and after stretch was calculated using the initial cross sectional area. The stress during the stress relaxation phase was evaluated using the normalized load. Since the strain is constant, the cross sectional area would remain constant and the stress decay can be evaluated effectively by measuring the change in load.

2.10 Impedance Calculations – Nyquist Plot

To measure the conductivity changes due to stress relaxation, the general performance of the circuit is needed to be known. Hence a more general circuit parameter such as impedance which considers factors other than just current and voltage has been employed in this modeling method to measure the resistance [40]. Electrochemical impedance which is the ability of a specimen to resist the flow of current is measured by applying a small sinusoidal voltage to the specimen and then measuring the current. The output AC current signal thus obtained was analyzed as a sum of sinusoidal functions (a

Fourier series) at the same frequency as applied voltage but shifted in phase. Thus the impedance is given by

$$\mathrm{Z} = \frac{Et}{It} = Eo\sin(\omega t)/\mathrm{Io}\sin(\omega t + \phi) = \mathrm{Zo}\sin(\omega\mathrm{t})/\sin(\omega\mathrm{t} + \Phi)$$

Where Z_o = Magnitude of Impedance and Φ = Phase shift

Using the Euler's relationship,

$$\exp(j\phi) = 2\cos(\Phi) + \mathrm{j}\sin(\phi)$$

Impedance can be represented as a complex number

$$\mathrm{Z}(\omega) = Zo * [\cos(\phi) + \mathrm{j}\sin(\phi)]$$

Generally the representation of the impedance spectrum as a function of frequency can be done in two ways namely the Nyquist and Bode plots [41]. A Nyquist plot is obtained by plotting the real part of Z (ω) on x-axis and imaginary part on y-axis (Figure 2.12) while a bode plot has two modes of representation: A modulus representation (log |Z| vs. log ω) which plots the magnitude of Impedance vs. the frequency and a phase representation (ϕ vs. log ω) which plots the phase angle vs. the frequency.

In this work, the Nyquist plot is used to represent the impedance spectrum of the specimen. From the Nyquist plot (Figure 2.13 shows a shape similar to EIS spectrum from the experimental data) it can seen that the low frequency data is towards the right side of the plot and the high frequency data is towards the left side of the plot which enables the membrane resistance (for liquid electrolytes this is called the solution resistance) to be determined easily [41].

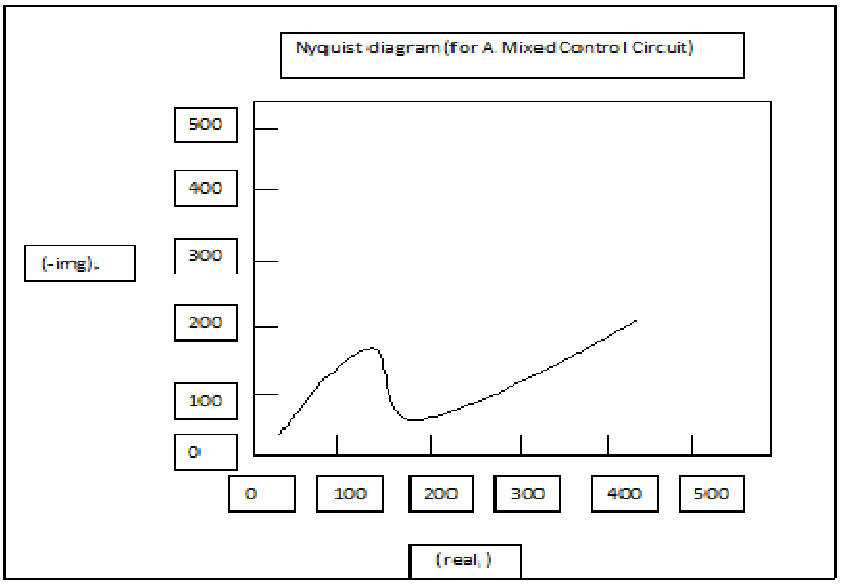

Figure 2.12 Sample Nyquist plot

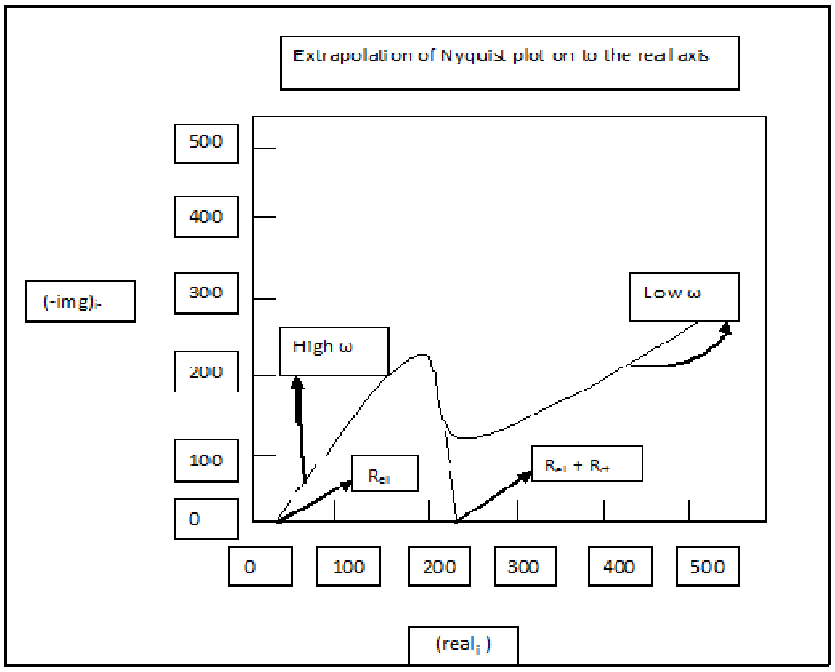

Figure 2.13 Electrolyte and charge transfer resistance in a Nyquist plot [41]

For a Nyquist plot, the impedance of the electrolyte is the point at which the left half of the semicircle touches the real axis and is obtained by extrapolating the graph onto the real axis (it is to be noted that each point on the plot is the impedance at one

frequency). The extrapolation of the graph onto the right side or the width of the semicircle gives the combined resistance of electrolyte and charge transfer impedance R_{ct} (R_{ct} is the impedance between the electrode and membrane which is a kinetically controlled electrochemical reaction). After determining the resistance of electrolyte from the Nyquist plot, the proton conductivity in the membrane is then calculated as

Conductivity k = 1/Z or R_{el}
Where Z or R_{el} = Resistance or impedance of the electrolyte
Thus the impedance at any time during the experiment was calculated by extrapolating the Nyquist plot on to the positive real axis.
The conductivity normalized using the formula
Normalized H^+ conductivity = k/kmax

In general, the conductance is given by σ = length /resistance*(width*thickness) is based off nominal dry thickness but since the conductivity was normalized every time, the parameters length and area (w*t) would get cancelled. Therefore these parameters were not used in calculation.

2.11 Equivalent Circuit Modeling

The analysis of EIS data was also performed by fitting an equivalent circuit model to the impedance data. The modeling of the circuit was accomplished based on the shape of impedance spectrum in the Bode and Nyquist plots. The EIS spectrum (modulus and phase data of the membrane) is shown in Figure 2.14.

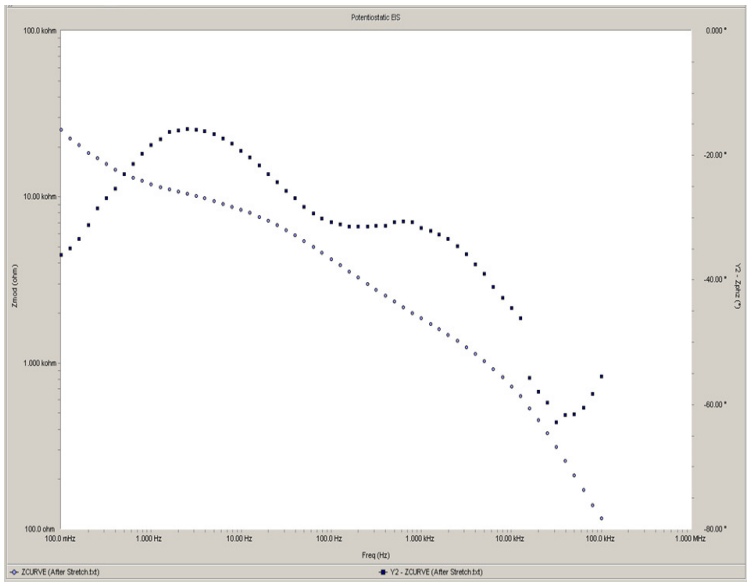

Bode plot, it can be seen that the modulus of the impedance is close to a straight line at 45 ° from the high frequency region towards the low frequency region while the phase plot followed an S-pattern. The ends of the impedance plot were considered as representative of the resistances as a whole and the contours as the capacitance. The line at an angle of 45° in the lower frequency region of Nyquist plot shown in Figure 2.15 can be modeled as the Warburg impedance element in the equivalent circuit. A Warburg element in a circuit occurs due to diffusion process and it depends on the frequency of potential perturbation [40]. Therefore at high frequencies, since the diffusing reactants do not have to move far, the Warburg impedance is small and at low frequencies the Warburg impedance is high as the reactants have to diffuse far.

The membrane comes in contact with the two electrodes from the impedance measurement device (the Teflon blocks with platinum wires and palladium foils) during an impedance test. Therefore, to account for the two electrode-electrolyte interfaces two double layer capacitances and a charge transfer resistance have been included in the

equivalent circuit. The resistance in the path between the electrodes is the electrolyte resistance. Since the Nyquist plot shown in Figure 2.15 shows a depressed semicircle with a diagonal line at an angle of 45°, a single Warburg element was added to the equivalent circuit model to account for diffusion at the interfaces.

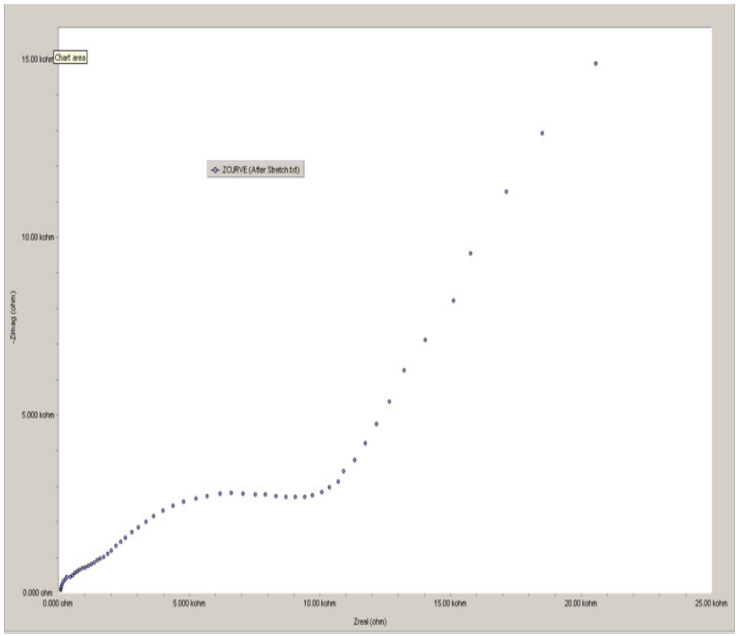

Figure 2.15 Nyquist plot (Z real vs. Z img)

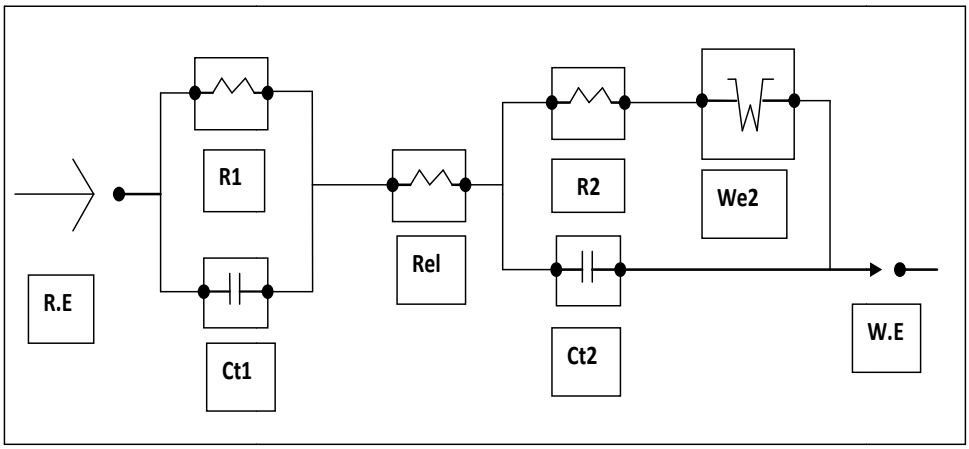

The equivalent circuit created is close to a battery model. The entire equivalent circuit is shown in Figure 2.16. The equivalent circuit is comprised of the following components: electrolyte resistance R_{el}, double layer capacitance C_t, Warburg impedance W along with charge transfer resistance R_i between the two layers. R1, Ct1, R2, Ct2 represent the in electrode/electrolyte interfaces since the cell operates in a two electrode mode while a single Warburg impedance element was enough to create a model for the current EIS spectrum.

The shape of the impedance spectrum is controlled by the electrical elements and the interconnections between them [41]. Each circuit element comes from a physical process in the actual cell and has characteristic impedance associated with it. The procedure to calculate the optimum values of the model required initial estimates for the different elements in the circuit. The resistances at the high and low frequencies were estimated as typical electrolyte and charge transfer resistances while the capacitances and Warburg elements were assigned default values from Gamry software. From the Bode plot, the impedance at high frequency was taken as an initial value for Resr. The low frequency impedance was taken as the sum of all three resistances ignoring the Warburg impedance temporarily. Using the initial estimate of Resr the sum of the other two resistances (Re1, Re2) were found. The range of frequency between which the impedance varied greatly was found and the midpoint impedance in this frequency range was plugged in as the total capacitive impedance. Since the two capacitors were combined in series, the seed value was doubled while plugging in the value for individual capacitor. A unit value was initially assigned to Warburg impedance. The seed values of the variables were adjusted to create the best possible agreement between the experimental data and the impedance performance of the equivalent circuit. This was accomplished by an iterative process inside the Echem Analyst software by Gamry. The values of the resultant resistances and conductance along with the fit have been summarized in Section 3.7 of Results and Discussion.

2.12 Prony Series – Modeling and Characterization

A visco-elastic stress relaxation model for a specified relative humidity and temperature has been developed in this project. The model is based on a Prony series and incorporates the effect of physical process on the relaxation process as well as the characteristic time associated with the stress relaxation. The initial model was modified to incorporate the effect of activation energy using the Arrhenius relationship which links the characteristic time to the absolute temperature. The time-dependent changes in the membrane have also been modeled using visco-elasticity theory. Under the visco-elasticity theory, the membrane is assumed to behave like a Maxwell model as shown in Figure 2.17, which can exhibit both steady state creep and stress relaxation. [20].

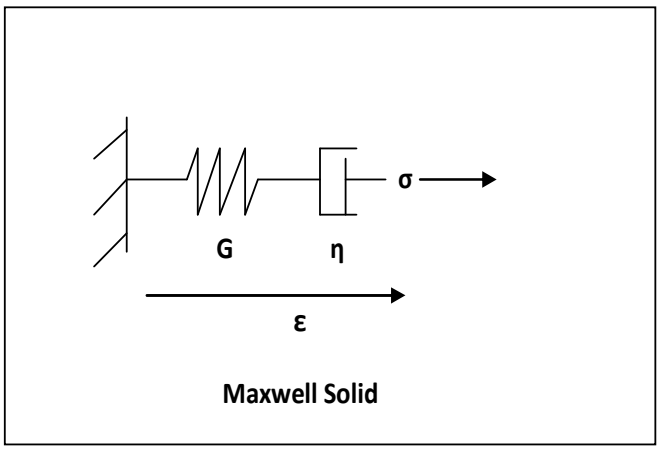

Figure 2.16 Maxwell solid

A Maxwell solid is a linear visco-elastic constitutive model which superimposes the constitutive equations of linear-elastic and viscous components [20]. The visco-elastic material properties are determined by creep or relaxation tests. In the current tests a relaxation test has been employed to measure the loading data. The time dependency of the relaxation modulus can be measured by subjecting the membrane to a step increase in strain and then measuring the resulting stress. Therefore in the current relaxation tests, after the application of initial load, the strain (ε_o) on the materials was held constant for experimentation time while the stress is recorded (Figure 2.18).

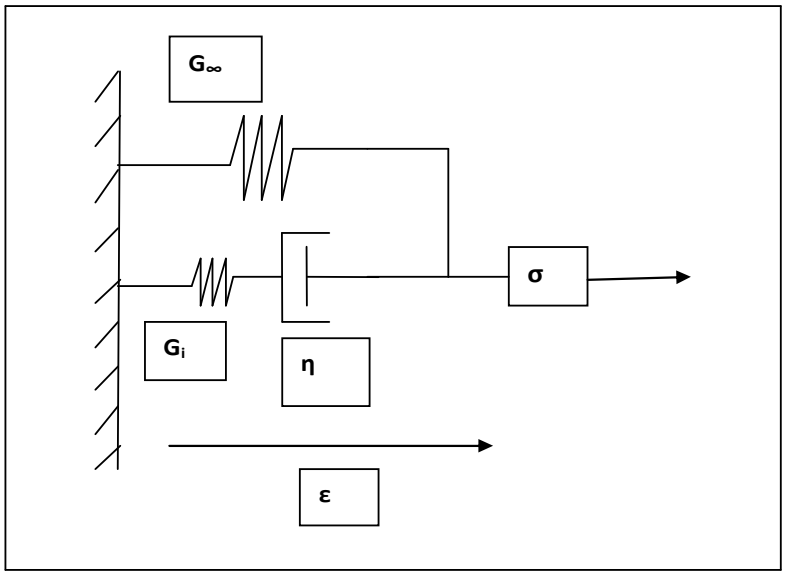

Figure 2.17 Modified Maxwell model

The Maxwell solid can be modified (adding a spring in parallel to Maxwell array of elements) to give a better fit for the response of polymer over longer periods of time. The modified Maxwell model (shown in Figure 2.18) comprises of a spring connected in parallel to the Maxwell elements in series. The relaxation modulus of the resulting element has the form shown in Equation 2.1.

$$\sigma = \{G\infty + \sum_{i=0}^{N} \mathrm{Gi} \exp(-\frac{\mathrm{t}}{\tau \mathrm{i}})\} \tag{2.1}$$

Equation 1: Response of the modified Maxwell model

Where G_∞ is the steady- state stiffness of the parallel spring

And G_i, t (*i,t = 1. . .N*) are the stiffness and time constants of the Maxwell elements.

The properties of the model are used directly as these parameters and the sum of the exponentials is known as the Prony series [43]. Thus a Prony series, a distribution of step functions (sum of exponentials) used to model the relaxation response behavior of the membrane. The net response (Equation 2.1) of the membrane was calculated by summing up the exponential terms along with the steady-state stiffness of the parallel

spring which represents the initial compliance of the membrane due to application of load.

A Prony series (Equation 2.2) which is commonly employed to model the visco-elastic stress relaxation behavior for membrane with multiple characteristic times is a mathematical form of representation of relaxation curves [11].

$$\sigma\,(t) = C1 * \exp(\frac{t}{(\tau 1)}) + C2 * \exp(\frac{t}{(\tau 2)}) + C3 * \exp(\frac{t}{(\tau 3)}) + C4 * \exp\left(\frac{t}{(\tau 4)}\right) + \sigma\infty \qquad (2.2)$$

Where C_i is contribution of physical process to the relaxation process

$\boldsymbol{\tau}_i$ is characteristic time associated with the relaxation process

σ_∞ is the equilibrium stress

To account for the temperature dependency of each process the mathematical curves can be simplified using the concept of activation energy. The resulting theoretical curves though do not a make a perfect fit for the experimental data at each temperature are much simpler to manipulate. The terms in the resultant theoretical representation can also be assigned a physical meaning. By the Arrhenius relationship, the characteristic decay time is dependent on temperature and is given by the relation

$$\frac{1}{\tau(T)} = \left(k * \frac{T}{h}\right) \exp(-\frac{Q}{R*T}) \qquad (2.3)$$

Equation 2.3 represents the Arrhenius relationship for a single exponential model. Where

k is Boltzmann's constant,

h is Planck's constant

R is Universal gas constant

T is Absolute temperature

And Q is Activation energy

Incorporating the Arrhenius relationship into each characteristic time of the stress equation, the stress relaxation function (Equation 2.4) becomes,

$$\sigma\,(t) = A * \exp(\frac{t}{\tau 1 * T}) + B * \exp(\frac{t}{\tau 2 * T}) + C * \exp(\frac{t}{\tau 3 * T}) + D * \exp(\frac{t}{\tau 4(T)}) + \sigma\infty \qquad (2.4)$$

Assuming the overall relaxation process to be temperature independent, the three activation energies can be determined for any constant temperature as shown in Equation 2.5.

$$\frac{1}{\tau i}(T) = \left(\frac{kT}{h}\right) * \exp(Qi / RT) \quad (2.5)$$

$$i = 1, 2, 3$$

Once the activation energies have been found the stress relaxation response for any particular temperature can be found. The results of Prony series modeled for different loading conditions along with their characteristic times and fitting R square values, activation energies are summarized in Section 3.7 of Results and Discussion.

3. RESULTS AND DISCUSSION

3.1 Results for Water Content of Nafion

The Nafion® specimens were subjected to two pre-treatments to estimate the time for water uptake. In the first test, the specimens were boiled in 0.5M sulphuric acid for one hour followed by boiling in DI water for one hour. In the second test the specimens were not subjected to any treatment. To find out the exact value of water content 'λ' in the membrane specimens, each specimen was placed in a closed chamber purged with water vapor saturated N_2 gas and the percentage of weight gain along with the time for weight gain were recorded for each set of specimens.

The data was recorded in two phases. In the first phase the weight gain due to pre-treatment was recorded (the membrane specimens were subjected to two different procedures shown in column 1 of Table 3.1). In the second phase the overall change in weight of the specimens when they were placed in the chamber and were exposed to vapor saturated N_2 gas was recorded.

Table 3.1 Percent weight gain for specimen subjected to different pre-treatments

Type of Treatment	% Change in weight after the test	% Change in weight when exposed to vapor N_2 gas after the test
Boiled in H_2SO_4 and DI water	4.5%	-4.5%
No Treatment (as received membrane)		2.13%

Table 3.2 Time taken for weight gain

Type of pre-treatment	Time taken for weight gain	Percent increase in relative humidity inside the chamber
No Test (as received membrane)	15 min	>25%
Boiled in H_2SO_4 and DI water for about 1 hour in each solution	9min	>20%

The time taken for weight gain of the specimens due to pre-treatment and when exposed to humidified N_2 gas was recorded. The membrane pretreated in sulphuric acid and de-ionized water (boiled in sulphuric acid for 1 hr followed by an hour in DI water) took less than 9 minutes to stabilize with the chambers environment showing no further increase in weight after 9 minutes (Table 3.2 lists the time taken for all three specimens). The membrane specimens subjected to no chemical pre-treatment took 40% more time when compared to specimen's subjected pre-treatment in sulphuric acid and DI water. The membrane sets pre-treated in sulphuric acid and DI water equilibrated with the chamber environment quicker due to presence of hydrophilic network and the membrane subjected to no pre-treatment took more time due to lack of hydrophilic network. Thus the wait time for the membrane pre-treated in sulphuric acid and DI water was found.

3.2 Repeatability and Reliability of Conductivity Measurement Test Cell

To ensure that the test cell produces consistent results, the repeatability and reliability of the impedance measurement test cell was evaluated. The repeatability of the conductivity measurement test cell was verified by repeating the test using the same test parameters and by changing the mode (Galvanostatic, Hybrid, and Potentiostatic) of impedance measurement. The reliability was verified by comparing the results obtained from similar experiments conducted on both the conductivity measurement test cell and sample cell.

3.2.1 Results of Repeatability

In order to test the repeatability a 20 X 60 mm sized specimen was cutout from as received Nafion® sheet and was installed between the grips. A Galvanostatic EIS technique was employed numerous times to measure the impedance of the same membrane (the results are of the tests are shown in Figure 3.1). In addition, the robustness of the test cell was verified by varying the user controlled input parameters of the impedance measurement technique and checking if the impedance measurements

remained the same for each test. For a Galvanostatic EIS technique the user controlled variables include AC current, frequency range, area and input impedance. As discussed earlier in Section 2.4, the Galvanostatic mode employs the application of current and measures the potential between the electrodes. For testing the robustness of the test cell, each of the input parameters was varied and the impedance was measured. Specifically, the AC current was varied from 0.0001 to 0.001 amp, frequency range was varied from 0.1, 1 to 100, 1000 KHz, input impedance from 100 to 1000 ohms and the areas (which are not used in measuring the impedance but are used for calculating conductivity) were varied as 1, 2, 2.5, 5, 25, 50 and 62.5 cm^2. Even with the variation of the input parameters there was no significant change in the measured impedance of the membrane. Also since the tests were conducted on the same membrane one after another, the repeatability of the conductivity measurement test cell was proven (Figures 3.2 and 3.3).

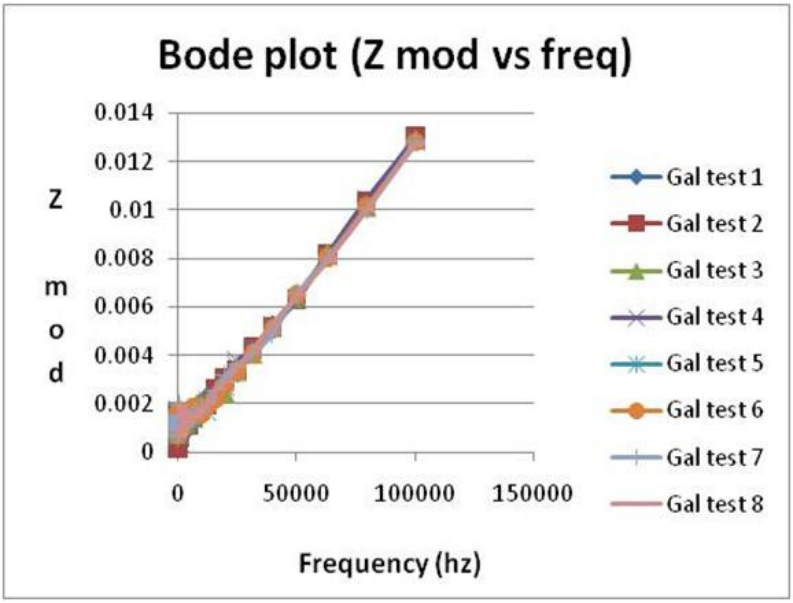

Figure 3.1 Galvanostatic tests for repeatability

Figures 3.2 and 3.3 show the results of the repeatability tests (where the only variable changed was the "area" which is used in computing conductivities, not used in measuring the impedance) and robustness where the control current was varied. The

impedance curves produced were very close to each other proving that the test cell yields consistent results for repeatable tests.

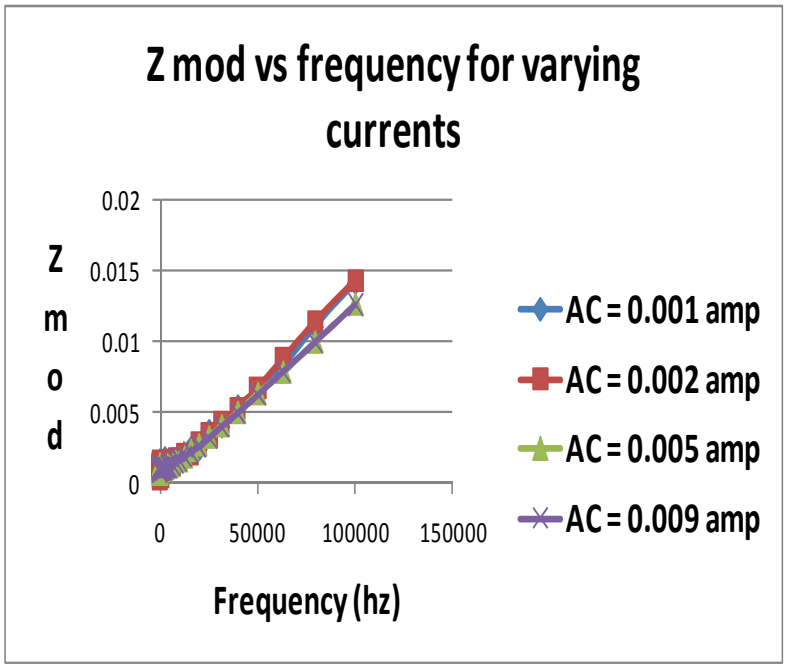

Figure 3.2 Tests for robustness

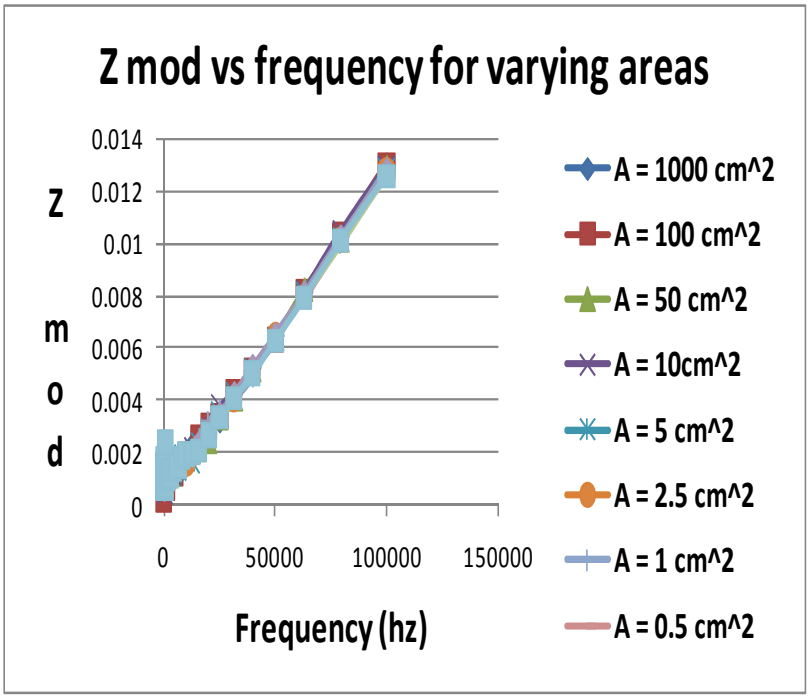

Figure 3.3 Impedance plot for varying input areas

3.2.2 Results for Reliability

To test the accuracy of the impedance measurement test cell, the as-received membrane was tested on two different impedance measurement test cells. The first test cell being the novel test cell integrated into the environmental chamber and then on an independent impedance measurement test cell.

The independent impedance measurement test cell had two square shaped Teflon blocks that came in contact with the membrane specimen from either ends. These Teflon blocks were bought in contact with the membrane manually. The blocks had provision for nuts and bolts in their corners that were locked after the membrane was placed between the electrodes. During an impedance test, the electrodes mounted on inner side of Teflon probes of test cell come in contact with the membrane from either ends. On one side of one Teflon probe, there were two platinum wires that ran parallel to each other. The other Teflon probe that came in contact with the membrane specimen had two palladium foils that also ran in a parallel fashion at 180 degrees to direction of platinum wires.

Impedance of the membrane was measured by connecting the input cables from a Gamry Potentiostat to the wires running out from the platinum wires and palladium foils of the Teflon probes. The Galvanostatic EIS technique that measures impedance by applying an AC input current and then measures the voltage across the electrodes was employed. An impedance test was conducted on an as received membrane at ambient conditions. Though the independent test cell was similar in design, the size of the Teflon blocks, palladium wires and platinum foils were much bigger in size (approximately two times) compared to chamber test cell. Thus during the impedance test the contact area of membrane with the electrodes varied in both the test cells.

A common EIS technique (Galvanostatic) with same input parameters (area, frequency range and current) was employed for both the test cells. After testing the membrane on the two test cells it was seen that both the test cells produced similar patterned results with a very slight variation in magnitude of the impedance (Figure 3.4).

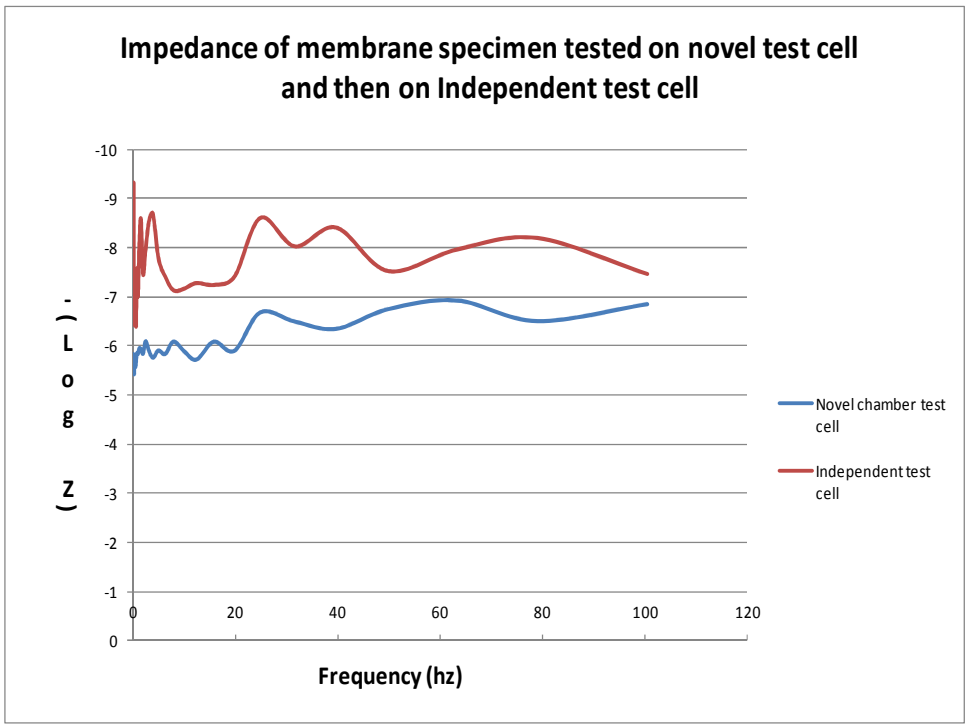

Figure 3.4 Impedance of membrane specimen tested on two test cells

Though similar input parameters and the same EIS technique were applied, the impedance curves for both the test cells were different but varied in a predictable manner. The average magnitude difference between the two impedance curves was 1.57 with a standard error of 0.122. The conductivity values could not be compared to literature or previous work as a base line experiment at 100% relative humidity could not be conducted due to technical difficulties. In future the test setup can be upgraded to allow the measurement of impedance membrane at 100% relative humidity which can accomplished by immersing the test cell along with the membrane in DI water. The difference in levels of impedance can be attributed to exposure of membrane to changes in environmental conditions while it is being transferred from independent test cell to chamber test cell. Thus the chamber test cell generated reliable results with the same EIS technique and while same input parameters being employed.

3.3 Comparison of Galvanostatic and Potentiostatic EIS Techniques Results

This section compares the results of impedance measured in two different EIS techniques namely Galvanostatic and Potentiostatic. For the Galvanostatic impedance test, an AC current of 0.005 amps was applied between the electrodes while the remaining input parameters like frequency range (0.1 to 100KHz), area (2.5cm^2), input impedance remained the same as Potentiostatic. In the Potentiostatic mode an input AC voltage of 10 mv rms was applied between the electrodes to measure the impedance. At ambient conditions, the membrane impedance was measured using both the techniques. At this temperature and relative humidity both techniques provided similar results. When the membrane impedance was measured during temperature control experiments, there was an overload signal in the Galvanostatic mode. The reason for this can be attributed to the method of the Galvanostatic impedance measurement technique. This mode applies a small current and then measures the potential between the electrodes through the membrane to calculate impedance of specimen. At low relative humidity's the membrane dries out completely resulting in a high resistance and hence higher current was required to produce a signal. Thus, the Galvanostatic EIS technique failed to measure the

impedance of dehydrated Nafion® as it produced zero voltage between the electrodes. Therefore, in order to study the changes in dehydrated Nafion® at varying hygro-thermal loads, the Potentiostatic EIS technique has been employed since the Potentiostatic technique applies a potential between the electrodes and then measures the current through the specimen. This mode prevents the equipment from encountering voltages that impose instability during the test and potentially damage the specimen.

The typical procedure for testing the Nafion membrane was as follows. The Nafion® which was pre-treated in sulphuric acid and stored in DI water was wiped with a kim-wipe to remove any liquid water before it was installed between the grips on the MTS 810. Approximately 25 minutes was allowed for the membrane to equalize with the chambers environment before conducting the first impedance test (the wait time was found from the water uptake experiments). The second impedance test was conducted immediately after stretching the membrane at a strain rate of 10mm/sec. The remaining impedance tests were conducted 20 minutes, one hour, and four hours after stretching the membrane. A set of three tests were conducted for each EIS technique**.**

3.4 Results from Stress Relaxation Experiments at Ambient Conditions

A set of five experiments were conducted to evaluate the stress relaxation behavior of the membrane at a constant 7% strain and ambient environmental conditions (30%RH and 27°C). After the membrane was installed, a time lapse of 20 min was allowed for the membrane to equalize with the chamber's environment before the stress was applied. The impedance of the membrane was measured before stretch, immediately after stretch, and at 20min, 1 hour and 4 hours during the stress relaxation phases. Figures 3.5 and 3.6 show the stress relaxation behavior of membrane for the first 500 seconds and for the entire length of the experiment. It was seen that the stress relaxed at a faster rate in the first few minutes when compared to the overall stress relaxation. The faster stress relaxation during the initial stage can be attributed to the rearrangement of polymer

chains due to release of load and further no application of additional load. It was found that the stress relaxed by 56% at ambient conditions.

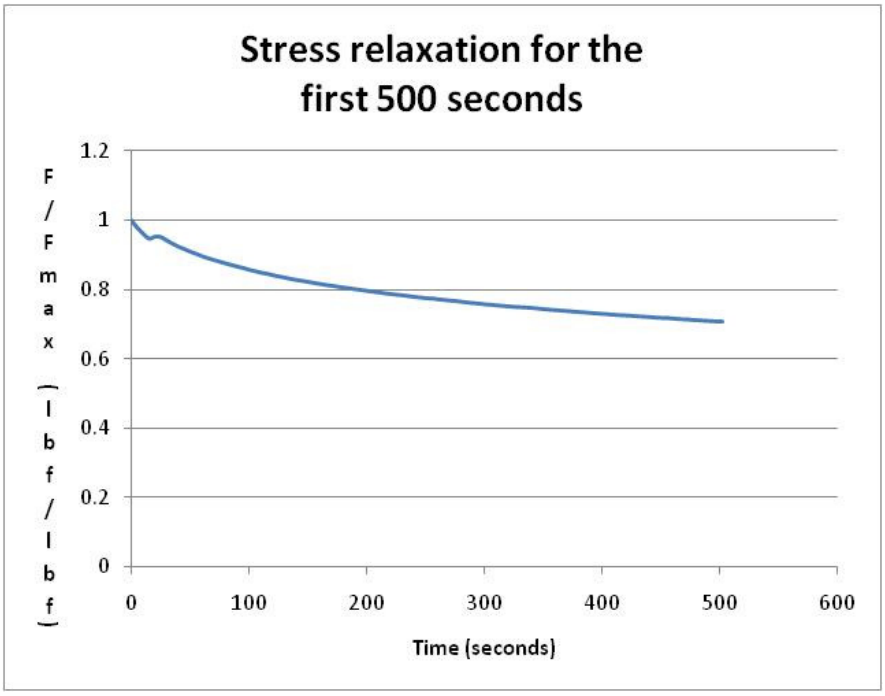

Figure 3.5 Stress relaxation immediately after stretch

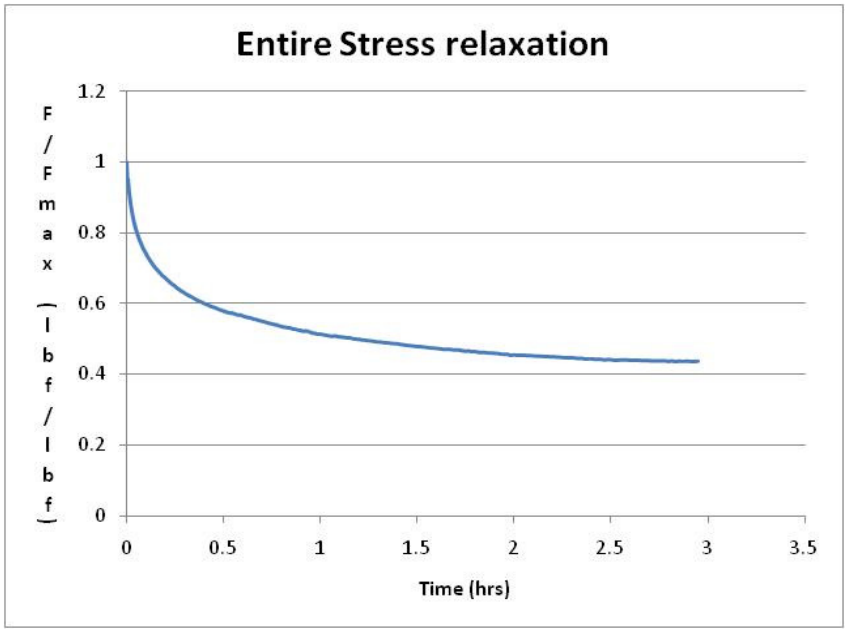

Figure 3.6 Stress relaxation before stretch, immediately after stretch, 1 hour and 2 hours after stretch at ambient conditions

Figure 3.7 shows the variation in proton conductivity of membrane when stretched at a constant strain and ambient conditions. The proton conductivity initially increased due to stretching, and then decreased during the stress relaxation phases. This phenomenon can be explained based on the morphological background of Nafion®. The increase in conductivity immediately after stretch indicates that the application of load causes a rearrangement of polymer chains. And once when the load was held constant, the overall stress reduced due to movement of inter-phase chains and adjustment of relative positions of bundles which facilitated easy proton transport [33]. During the stress relaxation phase, the polymer chains relaxed even further storing less amount of free water in the hydrophilic channel re-confirming that the pre-location of hydrophilic channels occurs at minimum water content as stated by Weber and Newman [31].

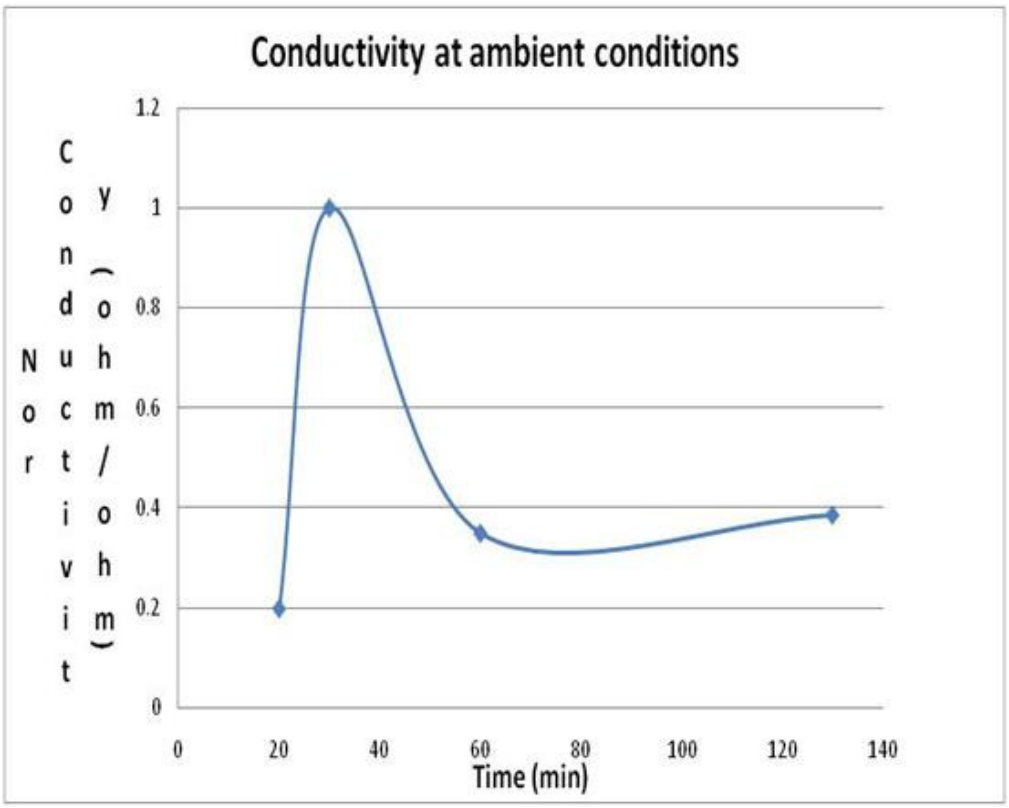

Figure 3.7 H^+ Conductivity of membrane before stretch, after stretch, 1 hour and 2 hours after stretch

Nafion® is composed of a fluorocarbon backbone which is hydrophobic in nature with sulphonic acid end groups which are hydrophilic in nature (the microstructure of Nafion® has been previously discussed in Section 1.4). Under the application of constant strain, the polymer chains readjust themselves before yielding and after yielding they disentangle and reorient [31]. At room temperature, due to existence of very few water molecules the stress relaxation behavior of membrane is dominated by the backbone structure of the membrane [15]. Consequently, when a constant strain is applied the length of hydrophilic channel in the polymer is reduced due to continuous chain disentanglements [15]. Therefore, the overall value of conductivity decreased exponentially with time reconfirming that when PEMs are stretched under constant strain the proton conductivity decays over time [32].

3.5 Results from Stress Relaxation Experiments with Temperature Variation

To test the changes in conductivity and stress relaxation of membrane with a variation in temperature, three sets of experiments were conducted. In each of these sets, the temperature inside the chamber was raised to the desired value (35˚C, 60˚C and 85˚C) before the stretching the membrane and the temperature was maintained at that desired value for the rest of the experiment. For the first set of experiments the temperature in the chamber was raised to 35°C before the stress relaxation experiment was conducted. In the second and third set of experiments the temperature inside the chamber was raised to 60°C and 85°C respectively before starting the stress relaxation experiments. After desired temperature was attained, the membrane was stretched at constant strain. The stress in the membrane was measured before stretch, after stretch and at 20min, one hour and four hour time-lapses during the stress relaxation phase at the three different desired temperatures. While Figures 3.8 and 3.9 show the temperature and relative humidity variation in the chamber during the course of experiment, the stress relaxation behavior of the membrane at the three different temperatures is shown in Figure 3.10.

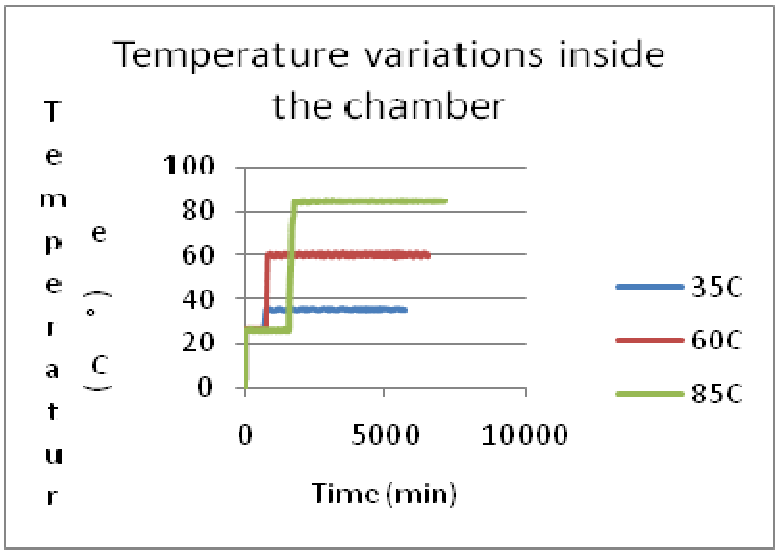

Figure 3.8 Temperature variations inside the chamber

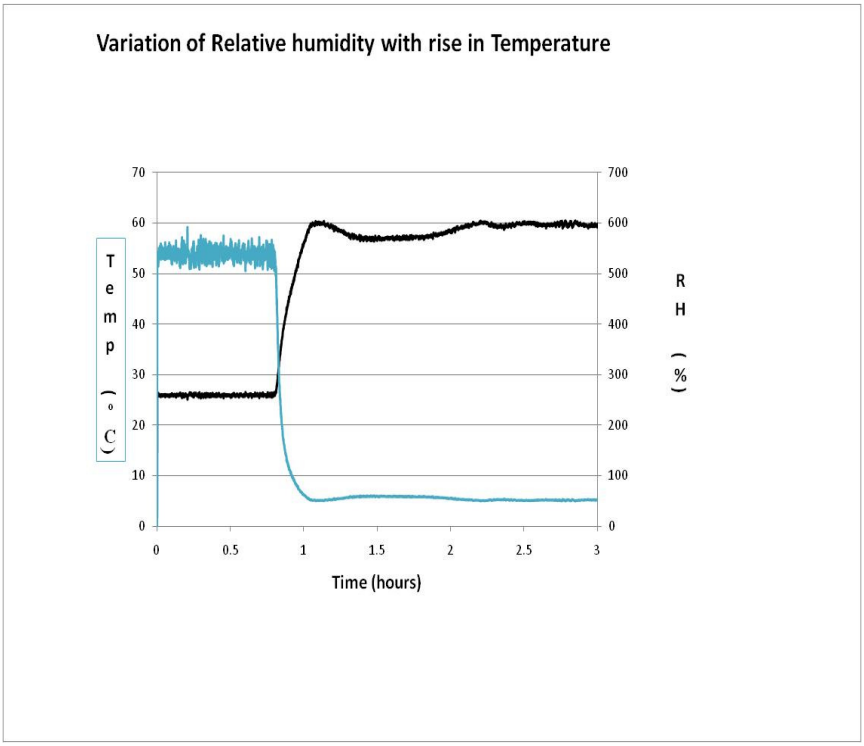

Figure 3.9 Variation of RH inside the chamber with a rise in temperature

From Figure 3.10, the rate of stress relaxation at both the elevated temperatures (35°C & 60˚C) was much faster when compared to ambient conditions (27˚C) (since the stress relaxation occurred during the first few minutes the time scale in Figure 3.10 for stress relaxation is shown only until 500 seconds). In addition the increase in temperature decreases the water uptake capacity. The decrease in the water uptake results in increased load carrying capability which causes this high percentage of stress relaxation [42]. At very high temperatures (85˚C) the polymer chain entanglements completely separate resulting in no measurable change in stress with the current load cell after loading the specimen. The mechanical integrity of the membrane is degraded significantly at high temperatures near 85˚C.

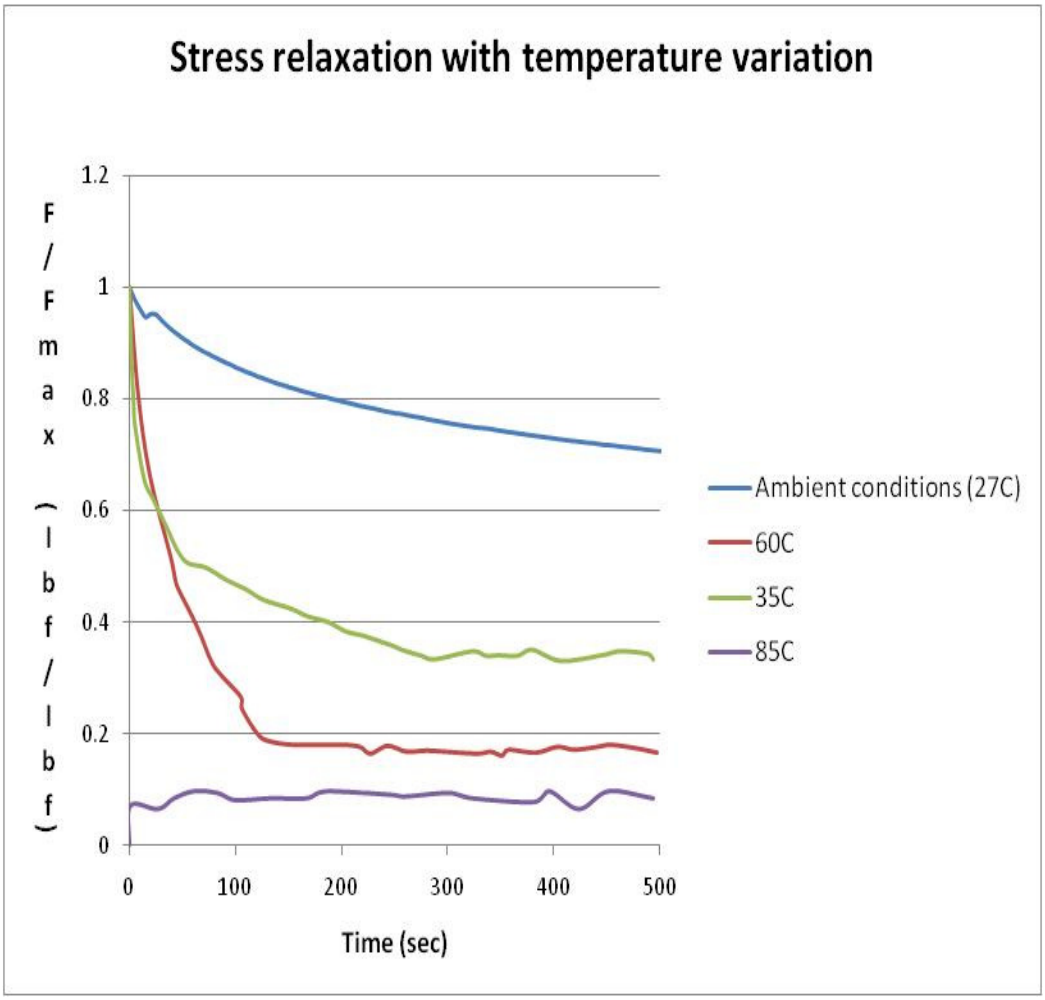

Figure 3.10 Stress relaxation of Nafion at 35°C, 60°C and 85°C for the first 500 seconds

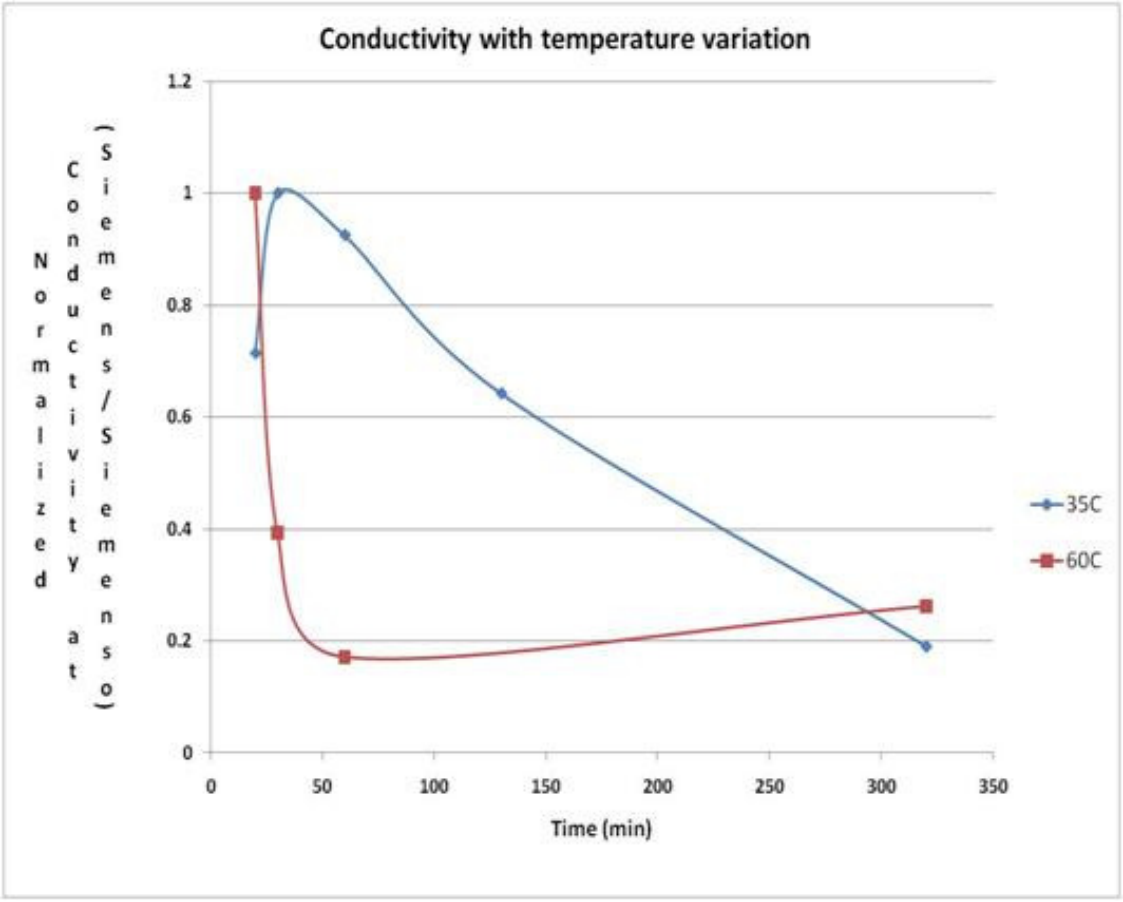

Figure 3.11 Proton conductivity at 35°C and 60°C

Figure 3.11 shows the changes in proton conductivity of the membrane at different temperatures during the stress relaxation. For the first set of experiments, when the temperature was raised from ambient conditions to 35˚C the conductivity increased after stretching and the absolute increase was proportional to the rise in temperature. This absolute increase in conductivity due to a rise in temperature can be explained in terms of combined effect of mechanical and hygro-thermal loading on the structure of Nafion®. When the membrane was exposed to high temperature (35˚C), humidity in the membrane decreased due to dehydration resulting in significant shrinkage of hydrophilic channels of the membrane which decreased the electrochemical conductivity of the membrane [8]. The membrane was also being held at constant strain along with the exposure to high temperature. The stretching of the membrane has caused rearrangement of polymer chains increasing the path of proton transport. This result is consistent with the result

obtained by Liu et al. in that the proton conductivity increased from un-stretched condition to stretched condition for a membrane completely immersed in water [15]. Later when the membrane was exposed to constant temperature of 35˚C during its stress relaxation phases, the conductivity decreased. The stress relaxation of the membrane have caused the ion channels to disperse widely decreasing the length of the proton transport network and also the lack of water at high temperature might have resulted in poor electrochemical conductivity [8].

In the second set of experiments, when the temperature was raised to 60°C there has been a decrease in conductivity initially from un-stretched state to stretched state. When a membrane is stretched the hydrophilic channels align themselves reducing the length of proton transport showing an increase in conductivity [15]. But there was a decrease in proton conductivity proving the interdependence of conductivity and water content [39]. When the temperature is raised, the water content in the membrane reduces as the hydrophilic domains shrink due to drying leading to a drop in conductivity. This decrease in conductivity from before stretching to after stretching and stress relaxation phase was observed at current high temperature (60˚C). Further, the slight increase in conductivity during the stress relaxation phases from after stretch phase indicates that at elevated temperatures (current temperature 60°C) relaxation process led to rearrangement of polymer chains reducing the length of proton transport. This phenomenon can also be explained based on morphological behavior theories of the membrane. Rubabat, Heijden, Gebel and Diat et al. [15, 34-37] have suggested that when a polymer electrolyte membrane is stretched, the polymer aggregates would initially rotate at low strains and they begin to disentangle and reorient when they reach high strains. From the bundle-cluster model, an application of small strain rotates the hydrophobic bundles which in turn lead to a more oriented hydrophilic channel along the direction of load thus reducing the length of proton transport [38]. The proton conductivity increases slightly even though the proton dissociation and diffusion coefficients (D_{σ}) do not change (which is due to same chemical structure).

It was difficult to make an estimate of conductivity for the stress relaxation experiments at the highest temperature (85˚C) as the Nyquist/Bode plots were not valid. Figure 3.12 shows the Nyquist plot of the impedance of the membrane at 85˚C. The shape does not follow a regular pattern (the standard pattern of Nyquist plot needed to calculate the impedance is shown in Section 2.10). At this high temperature, the membrane was physically and electrochemically degraded and did not record change in stress or support impedance measurements.

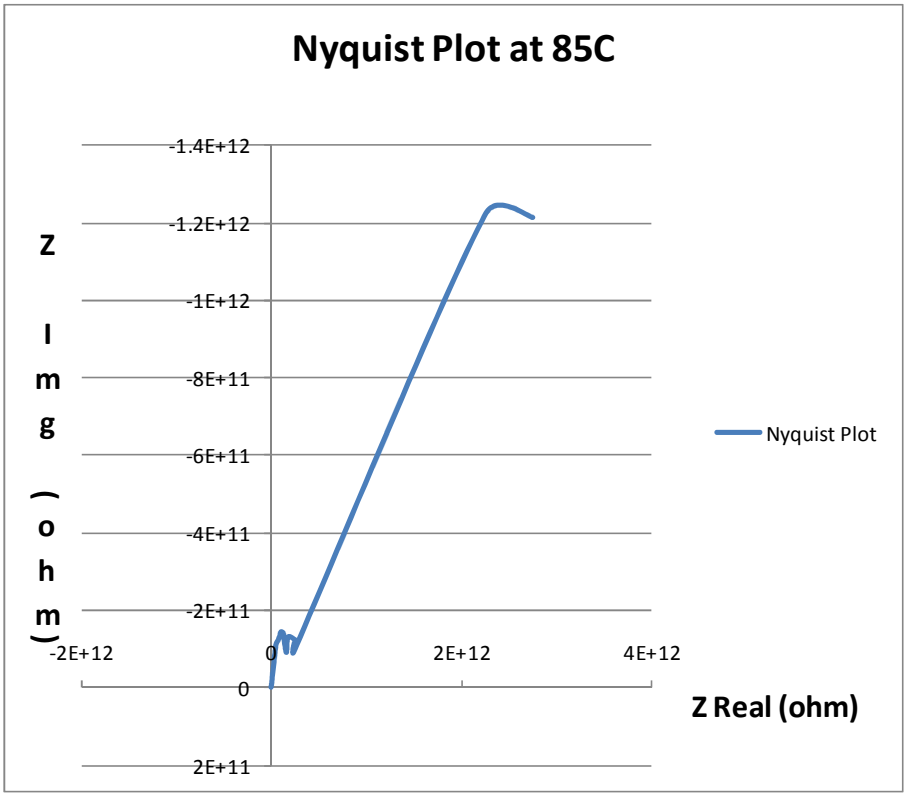

Figure 3.12 Nyquist plot at 85˚C

3.6 Results from Stress Relaxation Experiments with Relative Humidity Variation

Experiments that evaluate the effect of relative humidity cycling on the conductivity and stress relaxation of the membrane were conducted. In each of these experiments, the relative humidity inside the chamber was cycled by increasing or decreasing the current humidity value by 25 to 30% for varying dwell times as shown in Figure 3.13. The stress in the membrane was measured before stretch, after stretch and at every time the relative humidity was cycled at regular time intervals. The experiments differed by adjusting the dwell time at a specific humidity before the impedance measurement was taken. In the first experiment after varying the relative humidity a dwell time of 20 minutes was allowed for the membrane to equalize with chamber's environment before conducting the impedance test. In the second experiment, a dwell time of just 10 minutes was allowed before measuring the conductivity. Step increase/decrease in relative humidity was achieved by purging the chamber with dry and humidified N_2 gas (Section 2.5 describes the relative humidity set-up in detail).

Figure 3.13 shows the relative humidity cycling inside the chamber. The peaks in the relative humidity cycling were not stable which can be attributed to the manual control of humidity. Due to unstable peaks it was difficult to estimate the effect of relative humidity cycling on the stress relaxation of the membrane. Therefore the data obtained from the stress relaxation experiments could not be used for the development of a mathematical model. A new humidity control method is currently being implemented.

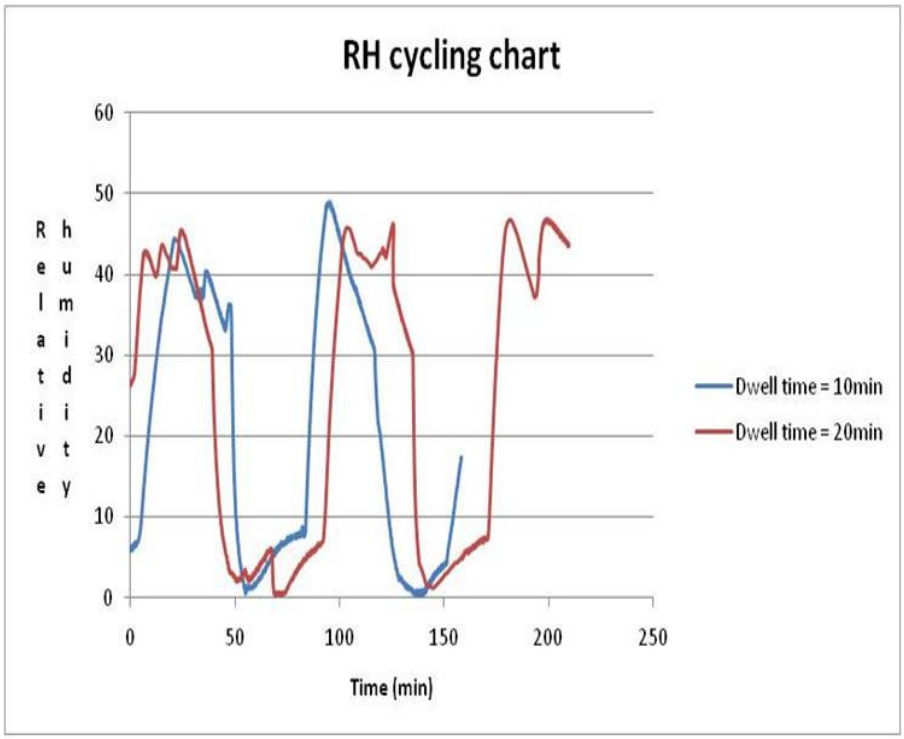

Figure 3.13 Relative humidity cycling inside the chamber

3.7 Equivalent Circuit Modeling – Results

The equivalent circuit used to model the experimental data is comprised of the electrolyte resistance, the charge transfer resistances between the interface of membrane and electrode, and the Warburg impedance. Figure 3.14, shows the diagram of the equivalent circuit. Two double layer capacitances were added to the charge transfer resistances for the interface resistance between the electrode and electrolyte to model the data in a better way. The equivalent circuit modeling was done for all the impedance tests and an example of data values from one of the tests is shown in Table 3.3. Figures 3.15 and 3.16 show the equivalent circuit fit for both Bode and Nyquist spectrums plotted from the experimental data.

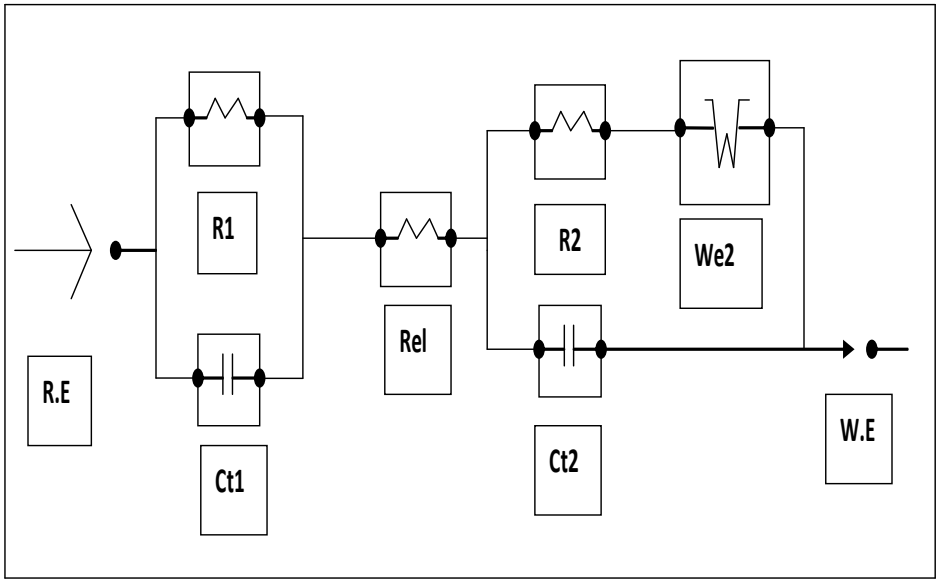

Figure 3.14 Equivalent circuit of the EIS spectrum

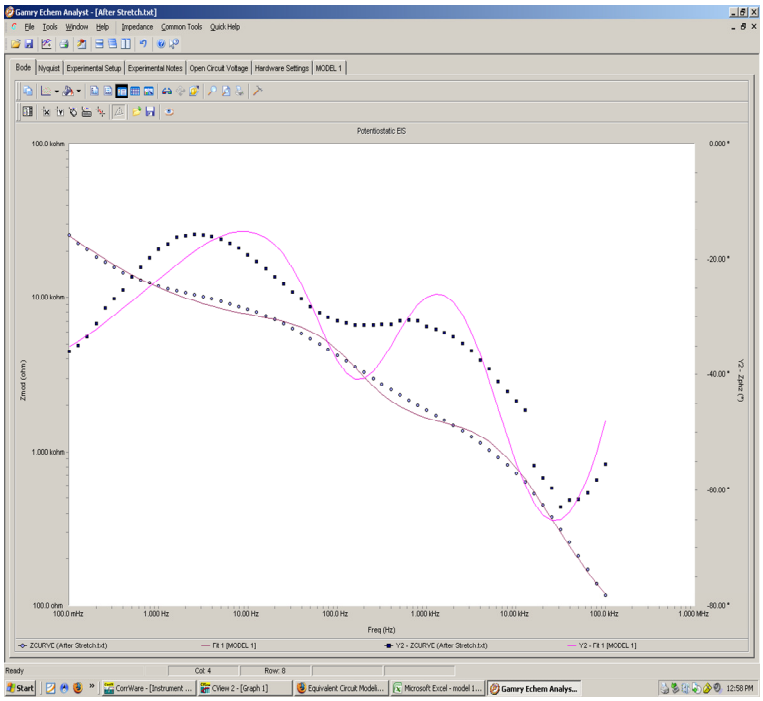

Figure 3.15 Equivalent circuit fit for the Bode plot

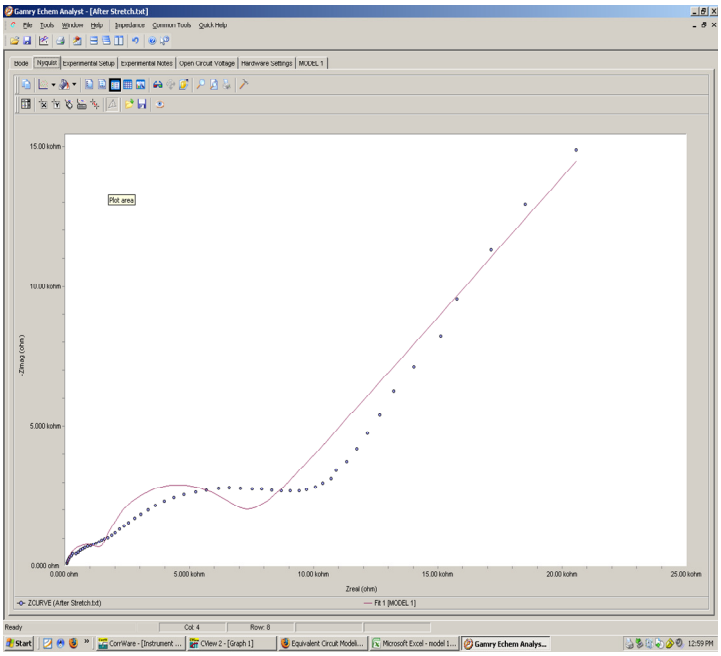

Figure 3.16 Equivalent circuit fit for the Nyquist plot

Table 3.3 Equivalent circuit parameter values at ambient conditions

Circuit Parameter	Optimum value	Error	Unit
Rel	74.3	2.23	Ohms
Re1	1.32E+03	16.54	Ohms
Re2	4.73E+03	69.25	Ohms
Ct1	1.86E-08	2.06E-10	F
Ct2	4.30E-07	9.32E-09	F
We2	6.16E-05	8.85E-07	S*s^(1/2)
Goodness of fit	13.99E-03		

3.8 Prony Series Modeling – Results

The visco-elastic stress relaxation response of the membrane with multiple characteristic times has been modeled using Prony series. In case of stress relaxation experiments with temperature control the effect of temperature was incorporated into the model using the concept of activation energy associated with each process (incorporation of Arrhenius relationship is explained in detail in Section 2.12). Prony series for different loading condition (stress relaxation with temperature variation along with ambient conditions) are summarized below.

At ambient conditions, 27ºC:

$$\sigma(t) = 0.1874 + (0.0159 * e^{0.4609t}) + (0.3365 * e^{0.0096t}) + (0.1134 * e^{0.0004t})$$

At 35ºC:

$$\sigma(t) = 0.3194 + (0.1635 * e^{0.219t}) + (0.3404 * e^{0.0086t}) + (2.8438 * e^{0.0128t})$$

At 60ºC:

$$\sigma(t) = 0.1781 + (0.633 * e^{0.2135t}) + (0.0001 * e^{0.0128t})$$

And the activation energies that were found to fit the data are listed in Table 3.4.

Table 3.4 Activation Energies for each temperature

'τ'	**Activation Energy, Q (KJoule/Mole)*Kelvin**
τ_1	79.797
τ_2	92.044
τ_3	101.022

The simplex search method was used to optimize parameters for the Prony series. Ordinary least squares method was then employed to determine significance of coefficients for the series**.** A three characteristic times 'τ' for the Prony series model was built for each experimental condition. From the modeled Prony series the increasing temperature causes faster stress relaxation reiterating the effect of temperature on the degradation of the membrane. The predicted model fitted very closely to the experimental data and the three term Prony series sufficiently explains the experimental data. The R-squared values also show the closeness of the fit. Table 3.5 lists the optimum 'τ' values along with the equilibrium stress values at each temperature condition

Table 3.5 Optimum τ values along with equilibrium stress for Prony series at all loading conditions

Type of Experiments	**τ_1 (1/sec)**	**τ _2 (1/sec)**	**τ _3 (1/sec)**	**σ∞(lbf/lbf)**
NIA	0.4609	0.0096	0.0004	0.1874
NI35	0.219	0.0086	0.0128	0.3194
NI60	0.2135	0.0128		0.1781

The plots shown in Figure 3.17 show the accuracy of predicted model with actual stress relaxation data. The data in the charts shows the normalized stress with time for both the experimental and modeled data. In order to study the stress decay in the membrane the load was normalized as at constant strain the cross-sectional area would remain constant (the details of evaluation of stress relaxation data is presented in Section 2.9, and NIA, NI35, NI60 stand for normalized load data at ambient, 35˚C, 60˚C respectively). The trend from NIA to NI60 shows a decline in decay rates as temperature increases. The‘t’ statistics of at least one exponential term are significant in all cases and ‘R’ square values along with the former prove the goodness of fit.

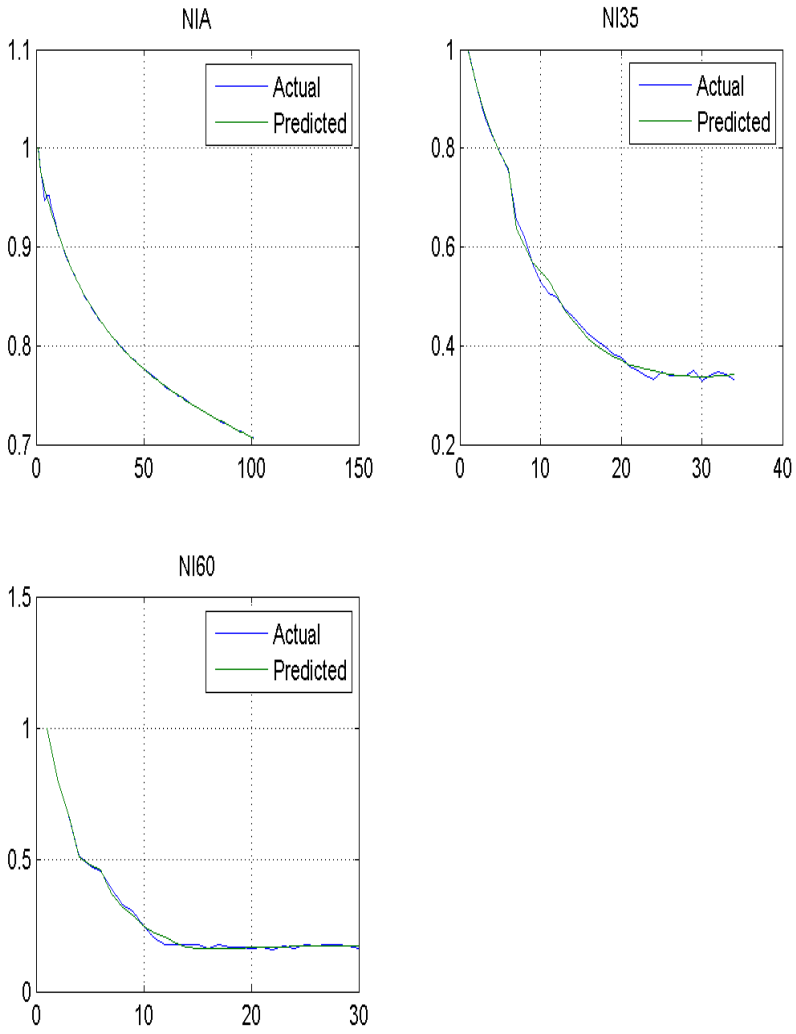

Figure 3.17 Prony series fitting of stress relaxation data

The Prony series was modified to account for temperature dependency using Arrhenius relationship. The Arrhenius relationship utilizes the concept of activation energy to account for the temperature dependency. After finding the activation energies, in order to find the optimal 'τ' and temperature, a least square fitting was done for the actual 'τ''s (determined above) against temperature. A sample of a regression fit is shown in Figure 3.18.

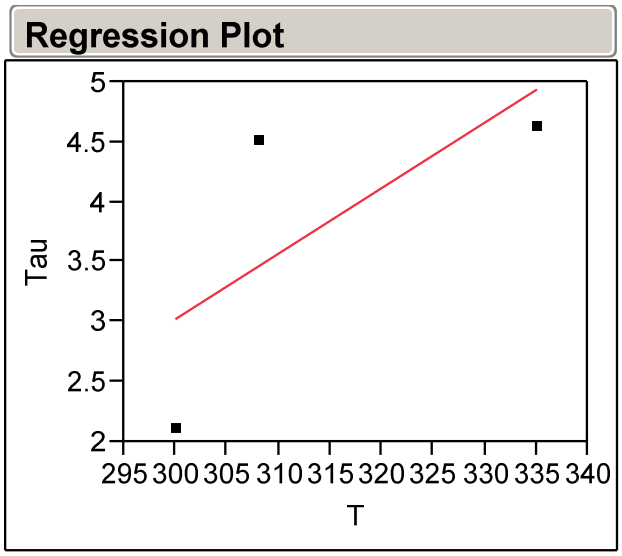

Figure 3.18 Sample Regression plot

The predicted values of 'τ' obtained from the regression fit were used to fit the experimental stress relaxation data. The fit at different temperatures is shown in Figures 3.19, 3.20 and 3.21. The predicted 'τ''s for the temperature did not fit the experimental data for the room temperature data well which indicates that additional mechanisms may be involved in the degradation of the membrane at this low temperature and warrants further study. Hence an optimum temperature for which the predicted 'τ''s would fit the experimental data is yet to be determined.

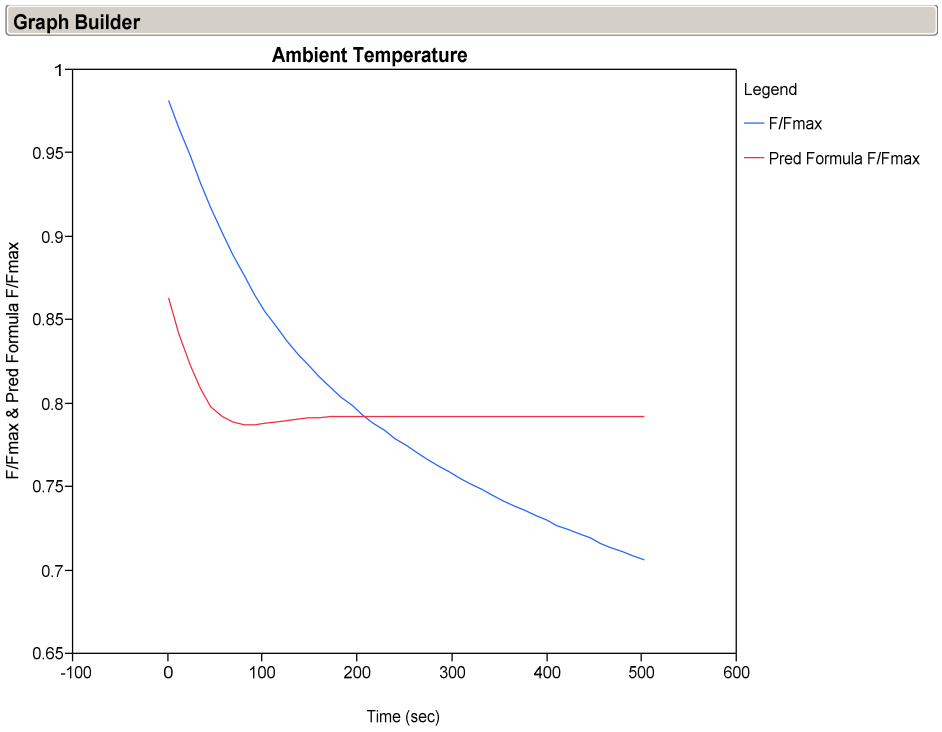

Figure 3.19 Predicted fit at ambient (27°C) conditions

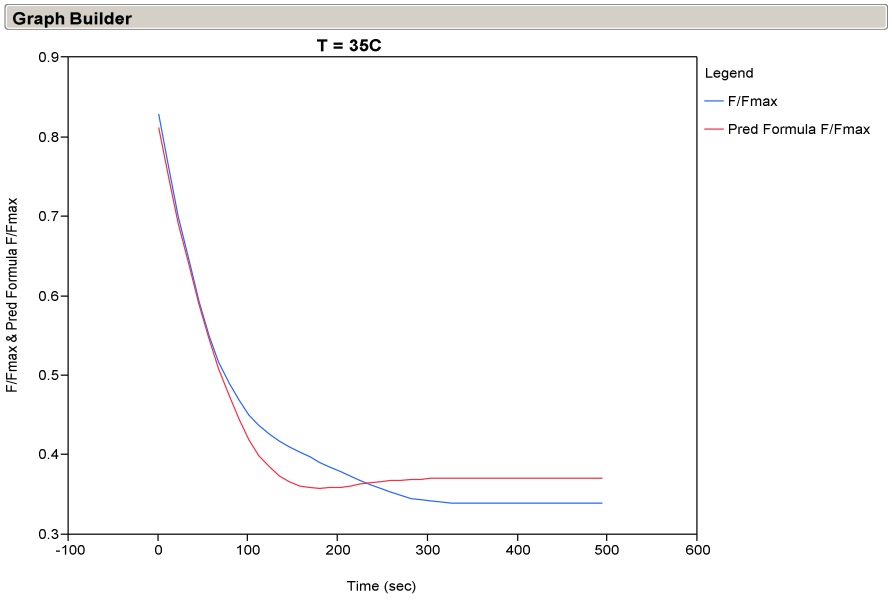

Figure 3.20 Predicted fit at 35°C

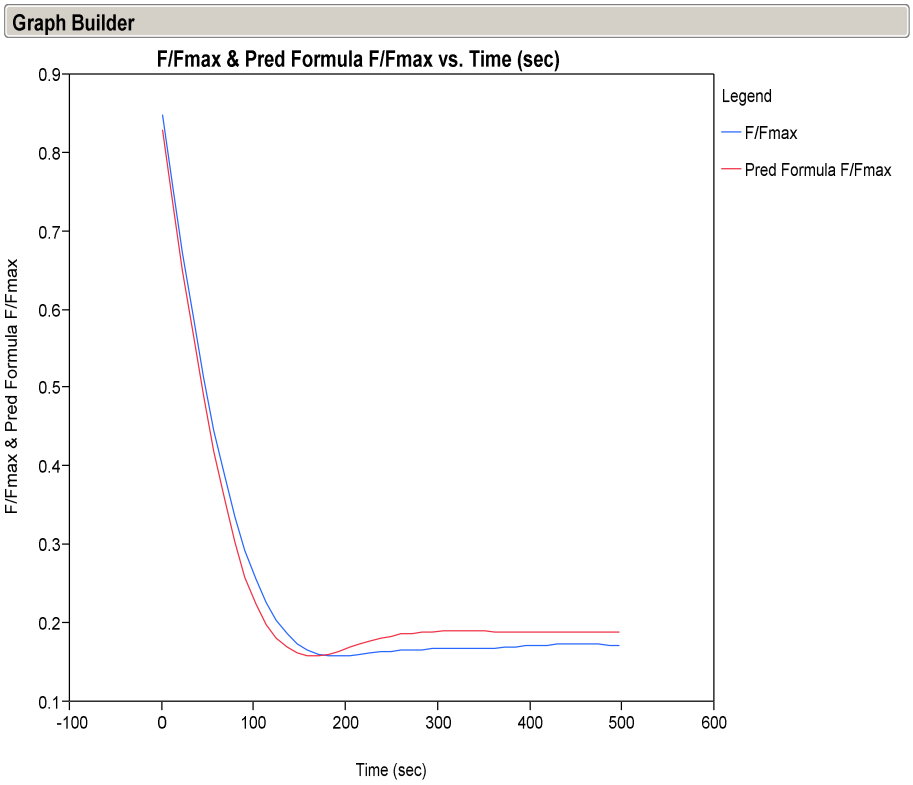

Figure 3.21 Predicted fit at 60°C

4. CONCLUSIONS AND FUTURE WORK

4.1 Conclusions

The experimental facility created to evaluate the electrochemical and mechanical properties of the Nafion® membrane was designed and fabricated. The equipment yielded consistent results that help to explain the degradation properties of Nafion®. The effect of mechanical and hygro-thermal loading on the proton conductivity of the membrane has been demonstrated and the interdependence of conductivity and stress relaxation on temperature has been shown in the experimental data. The stress relaxation behavior of membrane under various loading conditions provides a means to understand the behavior of membrane in an actual fuel cell. The results show the effect of temperature on the stress relaxation of membrane.

A visco-elastic stress relaxation model that incorporates the effect of physical process and temperature has been developed. The model results showed that with an increase in temperature the stress relaxes at a faster rate. The closeness of the predicted model with the actual stress relaxation data indicated that the model developed was accurate. The model (Prony series) which was initially developed for a particular temperature, relative humidity and temperature was later modified to incorporate the effects of activation energy. The room temperature stress relaxation data did not fit well with the activation energy concept and warrants further investigation. The conductivity curves could effectively predict the relation between temperature and water network in the membrane. As expected, the conductivity of membrane decreased with an increase in temperature.

The stress relaxation experiments at highest temperature and with relative humidity cycling did not yield reliable results. Further experiments are needed to predict the effect of relative humidity cycling on the stress relaxation behavior of membrane. It is also important to determine the cut-off temperature beyond which the membrane is degraded to such an extent that it does not allow proton transport.

4.2 Recommendations for Future

More work can be done using the current testing method in the future to get a better understanding of the degradation behavior of proton exchange membranes and build models to predict membrane life. The suggested future work is listed below.

- Variation of Mechanical loading:

The current work utilized one constant strain rate to study the stress relaxation behavior; the current facility can further be used to study the degradation properties for multiple strains. It is important to understand the behavior of membrane for more than one strain rate under hygro-thermal loading conditions, in order to predict the degradation properties more effectively as the morphology of the polymer is altered due to mechanical loading along with hygro-thermal conditions. Also the stress or load applied can be varied over time to analyze the membrane for varying stress histories. The current facility up can be used to conduct experiments for constant and varying strain, stress rates which help to analyze the time dependent behavior of membrane that help to determine the visco-elastic properties of the membrane.

- Effect of Hygro-thermal loading:

In the current project, though the membrane was subjected to relative humidity cycling with two different dwell times (20 min and 10min) consistent results were not obtained. In future work, the equipment can be upgraded to automatic relative humidity cycling setup and the effects of relative humidity variation on the stress relaxation behavior of membrane can be found (a specific value of relative humidity can be maintained throughout the experiment and its effect can be studied). Also the dwell time

of relative humidity cycling (greater dwell times) can be varied and its effect can be studied.

- Variation of boundary conditions:

The boundary conditions can be modified as the membrane in an actual fuel cell is compressed in more than one direction. Loading can be applied in more than one direction and loading effects along with other constraints be studied on the behavior of membrane. The geometry of the membrane can also be varied and the effects of the same loading conditions can be studied.

- Relative Humidity cycling

The changes in the impedance of the membrane due to relative humidity cycling can further be investigated. Like the three different temperature variation (35°C, 60°C and 85°C) experiments , the changes in the impedance and stress relaxation at different humidity's can be modeled. Also the dwell times of the relative humidity can further be increased or decreased to study the conductivity and stress relaxation changes in the membrane specimen.

- Laser extensometry studies of the membrane

The chemical structure and microscopic propertied of the membrane subjected to mechanical and hygro-thermal loading can be analyzed using the current test-setup. The impedance measurement test cell can be brought into position when performing the conductivity study but can be retracted back when not in use. This feature of the test set-up is useful in removing obstructions from the view of the membrane. This will allow the projecting of laser beams on to the membrane through the glass window. The results of light scattering can be used to analyze the polymer chain movements, diffusion as well as relaxation behavior of the specimen.

- Scanning Electron Microscopic studies of the membrane

The membrane can be removed at any time interval during testing or after the completion of test and its morphological structure can be studied using Scanning Electron Microscopy. The studies help to analyze the polymer chain disentanglements caused due to current loading conditions.

- Mathematical modeling

In the current research project, a mathematical model for the stress relaxation behavior of membrane at constant strain under varying temperatures was developed. It is possible investigate fundamental analysis to improve upon the empirical Prony series modeling. The decay in conductivity changes can be modeled and the electrochemical changes can be combined with the mechanical changes.

LIST OF REFERENCES

LIST OF REFERENCES

[1] F. Barbir, *Fuel cells for clean power generation: Status and perspectives*, Springer Netherlands, 2009.

[2] R. Osakwe, "PEM fuel cells and Russia's Supply of Platinum – Trading one bottleneck for another," *Journal of Russian, East European, and Eurasian studies*, vol. 2, spring 2006.

[3] R. Solasi, Y. Zou, X. Huang, K. Reifsnider, and D. Condit, "On mechanical behavior and in-plane modeling of constrained PEM fuel cell membranes subjected to hydration and temperature cycles," *Journal of Power Sources*, 167, 366-377, 2007.

[4] S. Banerjee, and D. Curtin, "Nafion per fluorinated membranes in fuel cells," *Journal of Fluorine Chemistry*, 125, 1211-1216, 2004.

[5] J. Gangi, "Fuel Cells in Transportation Applications," www.fuelcells.org, 2004. Last accessed: June 15, 2010.

[6] G. Crawley, "Proton Exchange Membrane Fuel Cells," www.fuelcelltoday.com, 2006. Last accessed: June 10, 2010.

[7] H. Tang, S. Peikang, S. Jiang, F. Wang, and M. Pan, "A degradation study of Nafion proton exchange membrane of PEM fuel cells," *Journal of Power Sources*, 170, 85-92, 2007.

[8] A. Collier, H. Wang, X. Yuan, J. Zhang, and D. Wilkinson "Degradation of Polymer electrolyte membranes," *International Journal of Hydrogen Energy*, 31,1838-1854, 2006.

[9] "Collecting the history of fuel cells in Smithsonian Institution, Fuel cell history project," http://americanhistory.si.edu/fuelcells, 2010. Last accessed: June 12, 2010.

[10] C. Wirguin, "Recent Advances in per fluorinated ionomer membranes: structure, properties and applications," *Journal of Membrane Science*, 120, 1-33, 1996.

[11] A. Jones, and J. Malladi, "Simultaneous measurement of conductivity and stress in perfluorosulfonate membranes," Fuel cell conference, 2009.

[12] AB. LaConti, M. Hamdan, RC. Mc Donald, W. Vielstich, A. Lamm, and H. Gasteiger, *Handbook of fuel cells: fundamentals, technology, and applications,* Wiley, England, 2003.

[13] Y. Li, "*Experimental studies on mechanical durability of proton exchange membranes*," Dissertation, Virginia Polytechnic Institute, 2008.

[14] A. Kusoglu, A. Karlsson, M. Santare, S. Cleghorn, and W. Johnson, "Mechanical response of fuel cell membranes subjected to hygro-thermal cycle," *Journal of Power Sources*, 161, 987-996, 2006.

[15] L. Hickner, "Relaxation of proton conductivity and stress in proton exchange membranes," *Journal of Materials and Technology*, 128, 503-509, 2006.

[16] C. Gavach, G. Pamboutzoglou, M. Nedyalkov, and G. Pourcelly, "AC impedance investigation of the kinetics of ion transport in Nafion® perfluorosulphonic membranes," *Journal of Membrane Science*, 45, 37-53, 1989.

[17] "Nafion physical and chemical properties," www.permapure.com/tech-notes/key-concepts/nafion-physical-and-chemical-properties, 1972. Last accessed: June 5, 2010.

[18] U. Pasaogullari, "Polymer electrolyte fuel cell systems for special applications," in Connecticut Global Fuel Cell Center, University of Connecticut, Storrs, CT 06269, 2008.

[19] J. Kerres, "Development of ionomer membranes for fuel cells," *Journal of Membrane Science,* 185, 3-27, 2001.

[20] T. Chen, "Determining a Prony series for a visco-elastic material from time varying strain data," US Army Research Laboratory, Vehicle Technology Directorate, Langley Research Center, Hampton, Virginia, Tech Rep. TR- 2000-210123 ARL-TR-2206, May 2000.

[21] "Mechanics of solids," http://www.engin.brown.edu/courses/EN22, 2007. Last accessed: July 10th, 2010.

[22] "DuPont™ Nafion® PFSA membranes," www.Feulcells.dupont.com, 2009. Last accessed: June 12th, 2010.

[23] "Viscoelasticity," http://mail.vssd.nl/hlf/m028ch06.pdf, 2001. Last accessed: June 15th, 2010.

[24] "EIS 300™ Electrochemical Impedance Spectroscopy Manual," www.gamry.com. Last accessed: June 24, 2010.

[25] "Reference 600™ Potentiostat/Galvanostat/ZRA Operators Manual," www.gamry.com. Last accessed: June 24, 2010.

[26] "DOE (Department of Energy) Multi Year Research, Development and Demonstration of Planned Activities," www1.eere.energy.gov/biomass/pdfs/mypp.pdf, 2003. Last accessed: June 15, 2010.

[27] N. Otmani, A. Morin, S. Orio, L. Rouillon, G. Delette, J. Blachot, G. Gebel, and S. Besse, "Stresses in Nafion membrane during fuel cell operation," www.perso.ensem.impl-nancy.fr/oloview.Lottin/CD/FCHOTMA 10-09-57.pdf, 2009. Last accessed: June 15, 2010.

[28] A. Kusoglu, A. Karlsson, M. Santare, S. Cleghorn, and W. Johnson, "Mechanical behavior of fuel cell membranes under humidity cycles and effect of swelling anisotropy on the fatigue stresses," *Journal of Power Sources*,170, 345-358, 2007.

[29] Y. Lai, C. Mittlelsteadt, and C. Gittleman, "Viscoelastic stress model and mechanical characterization of perfluorosulfonic acid (PFSA) polymer electrolyte membrane, Proceedings of the 3rd International Conference on Fuel Cell Science, Engineering and Technology," Ypsilanti, MI, May (23-25), 2005.

[30] "Nafion,"http://en.wikipedia.org/wiki/nafion. Last accessed: August 03, 2010.

[31] A. Weber, "Performance limitations and improvements of small-scale free-breathing polymer electrolyte membrane fuel cells," *J. J Electrochem Soc A*, 150:1008-1015, 2003.

[32] D. Liu, and M. Hickner, "Stretching Effect of Nafion Fibrillar Nanostructure," *J. J. J Engineering Materials-T ASME*, 40(26): 9455-9462, 2007.

[33] D. Liu, S. Kyriakies, S. Case, J. Lesko, Y. Li, and J. McGrath, "Tensile Behavior of Nafion and Sulphonated Poly (arylene ether sulphone) Copolymer Membranes and its Morphological Correlations," *Journal of Polymer Science*, 44: 1453-1465, 2006

[34] L. Rubatat, A. Rollet, G. Gebel, and O. Diat "Evidence of Elongated Polymeric Aggragates in Nafion," *Macromolecules*, 35, 45050-4055, 2002.

[35] L. Rubatat, G. Gebel, and O. Diat, "Fibrillar Structure of Nafion: Matching Fourier and Real Space Studies of Corresponding films and Solutions," *Macromolecules*, 37, 7772-7783, 2004.

[36] P. Heijden, A. Rosa, G. Gebel, and O. Diat, "Orientation of Drawn Nafion at Molecular and Mesoscopic Scales," *Macromolecules*, 37, 5327-5336, 2004.

[37] P. Heijden, A. Rosa, G. Gebel, and O. Diat, "Relaxation of Drawn Nafion Films studied with Birefingence Experiments," *Polymers for Advanced Technology*, 16,102-107, 2005.

[38] D. Liu, S. Kyriakides, W. Case, J. Lesko, Y. Li, and J. MacGrath, "Tensile Behavior of Nafion and Sulphonated Poly (arylene ether sulphone)," *Journal of Polymer science, Part B: Polymer Physics*, 44, 1453-1465, May 2006.

[39] D. Liu, S. Kyriakides, W. Case, J. Lesko, Y. Li, and J. MacGrath, "Copolymers and its Morphological Correlations," *Journal of Polymer Science, Part B: Polymer Physics*, 44, 1453-1465, 2006.

[40] V. Dam, G. Janssen and A. De Bruijin, "Review: Durability and degradation issues of PEM fuel cell components," *Fuel Cells*, 8, 3-22, 2008.

[41] "Gamry Manuals – Basics of EIS,"
www.gamry.com/app_notes/EIS_primer/basics_of _eis/pdf.
Last accessed: August 10, 2010.

[42] X. Zi, C. Song, H. Wang and J. Zhang, *Electrochemical Impedance Spectroscopy in PEM fuel cells Fundamentals and Applications*, Springer-Verlag, NY, December 2009.

[43] C. Ishiyama and Y. Higo, "Effect of humidity on Young's modulus in poly (methyl methaacrylate)," *Journal of Polymer Science. Part B: Polymer. Physics*, 40 (5), 460-465, 2002.

[44] A. Bower, "Applied Mechanics of solids, Constituent models – relation between stress and strain," http://solidmechanics.org/text/Chapter3_5/Chapter3_5.htm, 2008. Last accessed: Nov 13, 2010.